Frontiers in Bioscience Landmark

Front. Biosci. (Landmark Ed) **2026**; 31(7): 52064
https://doi.org/10.31083/FBL52064

Original Research

GPR19 Drives Cell Cycle Progression via ERK-Dependent FOXM1 Activation in p53-Mutant Breast Cancer

Jihan Qiu[1,†], Cheng Tian[1,†], Hanzhi Li[1], Sumei Gao[1], Chengcheng Yang[1], Qiuyan Luo[1], Yang Liu[1], Kuan He[1], Kang Li[1], Yang Peng[1], Haochen Yu[1], Lingfeng Tang[1,*], Shengchun Liu[1,*]

[1]Department of Breast and Thyroid Surgery, The First Affiliated Hospital of Chongqing Medical University, 400016 Chongqing, China
*Correspondence: telephoneme@sina.com (Lingfeng Tang); liushengchun1968@163.com (Shengchun Liu)
[†]These authors contributed equally.
Academic Editor: Jordi Sastre-Serra
Submitted: 19 March 2026 Revised: 4 June 2026 Accepted: 17 June 2026 Published: 24 July 2026

Abstract

Background: G protein-coupled receptor 19 (GPR19) is an orphan G protein-coupled receptor with emerging relevance in cancer; however, its role in breast cancer remains poorly understood. Given the high frequency of tumor protein p53 (TP53) alterations in aggressive breast cancer, particularly triple-negative breast cancer (TNBC), we investigated the clinical significance, biological function, and molecular mechanism of GPR19 in TP53-mutant breast cancer. **Methods:** Public datasets (Gene Expression Omnibus and The Cancer Genome Atlas) were analyzed to assess GPR19 expression in relation to TP53 status, molecular subtype, and prognosis. Expression was validated in breast cancer cell lines, paired clinical tissues, and tissue microarrays by quantitative PCR, Western blotting, immunofluorescence, and immunohistochemistry. Stable GPR19 knockdown models in MDA-MB-231 and BT-549 cells were used to evaluate proliferation, cell cycle distribution, and apoptosis. RNA sequencing, rescue experiments with the extracellular signal-regulated kinase (ERK) activator Ro 67-7476, and a nude mouse xenograft model were employed to investigate the underlying mechanism. **Results:** GPR19 was significantly upregulated in TP53-mutant breast cancer, primary tumors, and especially TNBC, and its high expression was associated with poor survival. Functionally, GPR19 depletion markedly suppressed cell proliferation, colony formation, and DNA synthesis, while inducing G2/M arrest and apoptosis in TP53-mutant breast cancer cells. Mechanistically, GPR19 knockdown reduced ERK phosphorylation and downregulated forkhead box protein M1 (FOXM1) and its downstream G2/M regulators cyclin B1 (CCNB1) and polo-like kinase 1 (PLK1), whereas total ERK levels remained largely unchanged. Pharmacological activation of ERK partially restored FOXM1 expression, alleviated cell cycle disturbance and apoptosis, and reversed the growth-inhibitory effects of GPR19 depletion. *In vivo*, GPR19 knockdown suppressed xenograft growth, reduced Ki-67 staining, increased terminal deoxynucleotidyl transferase-mediated dUTP nick-end labeling (TUNEL) positivity, and inhibited the ERK–FOXM1–CCNB1/PLK1 signaling cascade, all of which were partially rescued by ERK activation. **Conclusions:** GPR19 functions as a novel oncogenic driver and clinically relevant biomarker in breast cancer, particularly in TP53-mutant and TNBC subsets. By activating the ERK–FOXM1 axis, GPR19 sustains cell cycle progression and suppresses apoptosis, highlighting this pathway as a potential therapeutic vulnerability in aggressive breast cancer.

Keywords: G protein-coupled receptor 19; forkhead box M1; cell cycle checkpoints; p53 mutation; breast neoplasms

1. Introduction

Breast cancer remains the most frequently diagnosed malignancy among women worldwide and a leading cause of cancer-related death [1]. Although advances in molecular classification and systemic treatment have improved outcomes for many patients, breast cancer is still characterized by substantial biological heterogeneity, resulting in marked differences in aggressiveness, therapeutic response, and prognosis across subtypes [2,3]. Among these, triple-negative breast cancer (TNBC), defined by the absence of estrogen receptor, progesterone receptor, and human epidermal growth factor receptor 2 (HER2) expression, represents one of the most clinically challenging subtypes because of its high metastatic potential, frequent early recurrence, and limited treatment options [4]. Because established therapeutic targets are limited, finding novel molecular drivers of aggressive breast cancer remains crucial, especially for high-risk populations.

Alteration of the tumor protein p53 (TP53) gene is a defining molecular characteristic of aggressive breast cancer [5]. TP53 is one of the most frequently mutated tumor suppressor genes in human cancer and is particularly enriched in TNBC [6]. As a central regulator of genomic stability, p53 coordinates cell-cycle arrest, DNA damage responses, senescence, and apoptosis in response to cellular stress [7]. Loss or mutation of TP53 disrupts these protective mechanisms and enables tumor cells to evade apoptosis, tolerate genomic instability, and maintain proliferative capacity under conditions that would otherwise trigger growth arrest or cell death [8,9]. In breast cancer, TP53 alterations are strongly associated with poor prognosis, re-

sistance to therapy, and aggressive clinicopathological features [10]. However, although TP53 mutation is widely recognized as a hallmark of malignant progression, the signaling dependencies that sustain tumor growth in the TP53-mutant context remain incompletely understood.

In recent years, G protein-coupled receptors (GPCRs) have emerged as important regulators of cancer biology [11]. Beyond their classical role as membrane receptors that sense extracellular ligands, GPCRs are now recognized as dynamic signaling hubs capable of integrating microenvironmental cues with intracellular oncogenic programs [12]. Aberrant GPCR activation can result from receptor overexpression, altered ligand availability, constitutive receptor activity, or crosstalk with other receptor systems such as receptor tyrosine kinases [13]. Through these mechanisms, GPCRs influence a broad spectrum of malignant behaviors, including proliferation, survival, migration, invasion, metabolic adaptation, and therapeutic resistance [14,15]. Because GPCRs are highly druggable and constitute one of the most successfully targeted receptor families in pharmacology [16], increasing attention has been directed toward their potential value in oncology. Nevertheless, many orphan or insufficiently characterized GPCRs remain poorly explored in breast cancer, especially in genetically defined aggressive subtypes.

Among these receptors, G protein-coupled receptor 19 (GPR19) has gradually attracted attention as a potential cancer-associated molecule. Although its physiological functions and downstream signaling properties remain incompletely characterized, emerging evidence suggests that GPR19 may participate in tumor-related biological processes, potentially through its involvement in cellular stress responses and metabolic regulation [17]. In certain malignancies, GPR19 is overexpressed and associated with proliferative or invasive phenotypes. Previous work has linked GPR19 to cell cycle progression in lung cancer [18], whereas studies in breast cancer have suggested possible involvement in tumor plasticity and invasive behavior [19]. In addition, bioinformatics analyses have identified GPR19 as a candidate biomarker in melanoma and other tumors [20]. These findings suggest that GPR19 is a key, overlooked regulator of tumor progression; however, its expression pattern, clinical relevance, and functional role in breast cancer remain largely undefined.

A major biological feature of aggressive breast cancer is dysregulation of the cell cycle, especially at the level of checkpoint control and mitotic progression [21]. Sustained tumor growth depends not only on increased proliferative signaling but also on the ability of cancer cells to coordinate DNA replication, checkpoint surveillance, and mitotic entry [22]. In this setting, the G2/M transition is particularly important because it integrates mitogenic input with cellular responses to DNA damage and replication stress. Tumor cells that successfully maintain G2/M progression gain a considerable proliferative advantage, whereas disruption of this process can lead to cell cycle arrest or apoptosis [23,24]. Therefore, identifying upstream molecules that regulate G2/M-associated programs may provide important insight into the mechanisms that support breast cancer growth, especially in aggressive molecular contexts.

Two signaling components are especially relevant to this process: extracellular signal-regulated kinase (ERK) and forkhead box protein M1 (FOXM1). The mitogen-activated protein kinase (MAPK)/ERK pathway is one of the best-established mitogenic signaling cascades in breast cancer and acts as a central downstream effector of multiple receptor systems, including receptor tyrosine kinases and GPCRs [25]. Persistent ERK activation has been associated with enhanced proliferation, adaptive stress responses, and therapeutic tolerance [26]. FOXM1, a well-recognized oncogenic transcription factor, is a critical regulator of cell cycle progression and mitotic control [27]. It promotes the transcription of genes required for DNA replication, G2/M transition, and mitotic progression, including cyclin B1 (CCNB1) and polo-like kinase 1 (PLK1) [28,29]. FOXM1 is frequently overexpressed in breast cancer, particularly in aggressive subtypes such as TNBC, and has been linked to a poor prognosis and treatment resistance [30,31]. These observations suggest that signaling pathways capable of sustaining ERK activity and FOXM1 expression may play an essential role in maintaining malignant proliferation.

In this study, we defined the clinical significance and biological function of GPR19 in breast cancer, with a particular focus on the TP53-mutant setting. By integrating public dataset analyses, clinical specimen validation, loss-of-function experiments in TP53-mutant breast cancer cell lines, transcriptomic profiling, pharmacological rescue assays, and *in vivo* xenograft studies, we determined whether GPR19 is associated with aggressive breast cancer phenotypes and elucidated the signaling mechanism underlying its effects. Our study identifies GPR19 as a significant, underrecognized molecule in breast cancer, linking it to ERK-dependent FOXM1 signaling and cell cycle regulation, which sets the stage for future mechanistic and translational research.

2. Materials and Methods

2.1 General Study Design

This study was designed as a multistage investigation to define the clinical significance, biological function, and molecular mechanism of GPR19 in breast cancer. First, public datasets were analyzed to assess the association of GPR19 expression with TP53 status, molecular subtype, clinicopathological features, and patient prognosis. Second, GPR19 expression was validated in breast cancer cell lines and paired clinical specimens. Third, stable GPR19 knockdown models were established in TP53-mutant breast cancer cells to evaluate the effects of GPR19 on proliferation, cell cycle distribution, and apoptosis. Fourth, RNA

sequencing (RNA-seq) and ERK rescue experiments were performed to explore the underlying mechanism involving the ERK–FOXM1 axis. Finally, a nude mouse xenograft model was used to validate the functional role of GPR19 and the related signaling pathway *in vivo*.

2.2 Public Datasets and Bioinformatics Analyses

Public datasets were analyzed to characterize the expression profile and clinical relevance of GPR19 and FOXM1 in breast cancer. Tumor-versus-normal comparisons, TP53 mutational status analyses, molecular subtype stratification, and clinicopathologic association analyses were primarily performed using The Cancer Genome Atlas Breast Invasive Carcinoma (TCGA-BRCA) cohort and the Gene Expression Omnibus (GEO; GSE7101). The correlation between GPR19 and FOXM1 expression, as well as correlations involving selected cell cycle-related genes, was assessed using the built-in correlation analysis module of Gene Expression Profiling Interactive Analysis 3 (GEPIA3) based on TCGA-BRCA RNA-seq data. Survival analyses for GPR19 and FOXM1 were performed using the Kaplan-Meier Plotter platform based on publicly available breast cancer cohorts. Gene set enrichment analyses were performed using ranked gene lists and curated Hallmark gene sets, and perturbation-based hallmark enrichment analyses were performed using GPSAdb2.0 (https://www.gpsadb.com/) to assess the association of GPR19 and FOXM1 with proliferation-related programs, the G2/M checkpoint, E2F targets, and mitotic spindle signatures.

2.3 Clinical Specimens and Tissue Microarray

Ten paired breast cancer tissues and adjacent nontumorous tissues were collected from patients undergoing surgical resection at the First Affiliated Hospital of Chongqing Medical University. No patients received preoperative systemic therapy before tissue collection. Fresh tissues were used for RNA extraction and quantitative PCR (qPCR) validation. Matched formalin-fixed, paraffin-embedded specimens were used for immunohistochemical staining and tissue microarray-based assessment of GPR19 expression. All tissue collection and subsequent analyses were conducted in accordance with institutional ethical approval and written informed consent procedures.

2.4 Cell Lines and Culture Conditions

Human breast cancer cell lines MDA-MB-231 (ATCC HTB-26), BT-549 (ATCC HTB-122), MCF-7 (ATCC HTB-22), and BT-474 (ATCC HTB-20) were obtained from the American Type Culture Collection (Manassas, VA, USA). MDA-MB-231 and MCF-7 cells were maintained in Dulbecco's Modified Eagle Medium, whereas BT-549 and BT-474 cells were cultured in RPMI-1640 medium (Gibco, Waltham, MA, USA). All media were supplemented with 10% fetal bovine serum (ExCell, Dalian, Liaoning, China), 50 U/mL penicillin, and 50 µg/mL streptomycin. Cells were maintained at 37 °C in a humidified incubator containing 5% CO_2. Cell line authentication was performed by short tandem repeat profiling, and all cell lines tested negative for mycoplasma contamination before experiments. Cell line expression was validated using three independent biological replicates, unless otherwise specified.

2.5 Lentiviral Transduction and Generation of Stable Cell Lines

The single hairpin (shRNA) sequences targeting GPR19 and the non-targeting control shRNA were designed and synthesized by Tsingke Biotechnology Co., Ltd. (Beijing, China) using their commercial shRNA design service. Following annealing, the shRNA oligonucleotides were cloned into a commercial lentiviral shRNA vector supplied by Tsingke Biotechnology using Bacillus amyloliquefaciens strain H restriction endonuclease I (BamHI) and Escherichia coli strain RY13 restriction endonuclease I (EcoRI) restriction enzymes. Because this is a commercial vector and not an Addgene plasmid, there is no corresponding Addgene accession number. Positive clones were screened by colony PCR and verified by Sanger sequencing before lentivirus production. For RNA-seq, total RNA was extracted from short hairpin RNA negative control (shNC) and shGPR19 cells using TRIzol reagent, and RNA quality was assessed using the NanoDrop 2000 spectrophotometer (Thermo Fisher Scientific, Waltham, MA, USA) and Agilent 2100 Bioanalyzer (Agilent Technologies, Santa Clara, CA, USA) or LabChip GX system (Revvity, Waltham, MA, USA). RNA-seq libraries were prepared using the VAHTS Universal V6 RNA-seq Library Prep Kit for Illumina® (NR604-02; Vazyme, Nanjing, Jiangsu, China), purified with VAHTS DNA Clean Beads (Vazyme; N411-03), quality-checked using the Qsep-400 system (BiOptic Inc., City, Zhejiang, China), and quantified using the Qubit 3.0 fluorometer with the Qubit dsDNA HS Assay Kit (Thermo Fisher Scientific). Qualified libraries were sequenced on the Illumina NovaSeq 6000 platform using a paired-end 150 base pair sequencing strategy, with a mean sequencing depth of approximately 20 million clean reads per sample. Detailed shRNA sequence information is provided in **Supplementary Table 1**.

2.6 RNA Extraction and qPCR

Total RNA was extracted using the FastPure Cell/Tissue Total RNA Isolation Kit V2 (Vazyme). RNA concentration and purity were measured with the NanoDrop 2000 spectrophotometer (Thermo Fisher Scientific). Reverse transcription was performed using RT Master Mix for qPCR II (MedChemExpress [MCE], Shanghai, China). qPCR was carried out on the CFX96 system (Bio-Rad, Hercules, CA, USA) using the SYBR Green qPCR Master Mix (MCE). Relative gene expression levels were calculated using the $2^{-\Delta\Delta CT}$ method, with glyceraldehyde-3-phosphate dehydrogenase (GAPDH) as an internal control. Primer sequences are listed in **Supplementary Table 2**.

2.7 Protein Extraction and Western Blotting

Cells were lysed in lysis buffer (Beyotime, Beijing, China) supplemented with protease and phosphatase inhibitors (Beyotime). Protein concentrations were determined using a BCA protein assay kit (Beyotime). Equal amounts of protein were separated by sodium dodecyl sulfate polyacrylamide gel electrophoresis and transferred to PVDF membranes (Bio-Rad). After blocking, membranes were incubated overnight at 4 °C with the indicated primary antibodies, followed by incubation with appropriate horseradish peroxidase (HRP)-conjugated secondary antibodies. Protein bands were visualized using enhanced chemiluminescence substrate and quantified using ImageJ software (version 1.54, National Institutes of Health, Bethesda, MD, USA). GAPDH was used as the loading control, and phosphorylated (p-ERK1/2) was normalized to total ERK1/2 where indicated. Detailed antibody information is provided in **Supplementary Table 3**.

2.8 Immunofluorescence Staining

Cells were seeded onto glass coverslips, fixed in 4% paraformaldehyde, permeabilized with Triton X-100, and blocked in bovine serum albumin. Then, the samples were incubated with anti-GPR19 primary antibody overnight at 4 °C, followed by incubation with fluorophore-conjugated secondary antibody. Nuclei were counterstained with DAPI. Fluorescence images were acquired using a fluorescence microscope under identical exposure settings, and signal intensities were quantified using ImageJ software.

2.9 Immunohistochemistry and Terminal Deoxynucleotidyl Transferase-Mediated dUTP Nick-End Labeling Staining

Paraffin-embedded clinical tissues and xenograft tumor sections were subjected to immunohistochemical staining according to standard procedures. After deparaffinization, rehydration, antigen retrieval, and endogenous peroxidase blocking, tissue sections were incubated with primary antibodies against GPR19, ERK, p-ERK, FOXM1, CCNB1, PLK1, or Ki-67, followed by incubation with HRP-conjugated secondary antibodies and chromogenic detection. Hematoxylin was used for nuclear counterstaining. The proportion of positive cells, staining intensity, and H-scores were assessed using ImageJ software. Apoptotic activity in xenograft tissues was evaluated using a terminal deoxynucleotidyl transferase-mediated dUTP nick-end labeling (TUNEL) staining kit according to the manufacturer's instructions. Detailed dilution information for the antibodies used in immunohistochemistry is provided in **Supplementary Table 3**.

2.10 Cell Proliferation and Clonogenic Assays

Cell viability was assessed using the Cell Counting Kit-8 (CCK-8; MCE). Briefly, cells were seeded in 96-well plates and monitored over the indicated time period. At each time point, CCK-8 working solution was added, and absorbance was measured at 450 nm using a microplate reader. For 5-ethynyl-2′-deoxyuridine (EdU) incorporation assays, cells were incubated with EdU, fixed, permeabilized, and subjected to the Click-iT reaction according to the manufacturer's instructions (Beyotime, Shanghai, China). The proportion of EdU-positive cells was determined by fluorescence microscopy or flow cytometry, as indicated. For colony formation assays, cells were seeded in 6-well plates at a low density and cultured for approximately 10–14 days. Then colonies were fixed, stained with crystal violet, photographed, and counted using consistent size thresholds. For the cell proliferation assay, each time point was measured using three technical replicate wells. The EdU incorporation and colony formation assays were independently repeated three times.

2.11 Flow Cytometry for Cell Cycle and Apoptosis Analysis

For cell cycle analysis, cells were fixed in 70% ethanol at 4°C, treated with RNase A, and stained with propidium iodide (PI). Flow cytometric data were acquired using a FACSCalibur flow cytometer (BD Biosciences, San Jose, CA, USA). Cellular debris was first excluded based on forward- and side-scatter characteristics, followed by the exclusion of cell aggregates and doublets to obtain the singlet-cell population. The DNA content of singlet cells was displayed as a PI-A fluorescence histogram and analyzed using FlowJo software (FlowJo, LLC, Ashland, OR, USA). Cells with approximately 2N DNA content were classified as G0/G1-phase cells, cells with DNA content between 2N and 4N as S-phase cells, and cells with approximately 4N DNA content as G2/M-phase cells. For apoptosis analysis, cells were collected using EDTA-free trypsin and stained with Annexin V–fluorescein isothiocyanate (FITC) and PI using a commercial apoptosis detection kit (BioLegend, San Diego, CA, USA), followed by immediate flow cytometric analysis. Cellular debris and aggregates were sequentially excluded, and the singlet-cell population was analyzed using compensated Annexin V-FITC fluorescence on the y-axis and PI-associated fluorescence recorded in the PerCP-Cy5.5-A channel on the x-axis. Annexin V-FITC−/PI− cells in Q4 were defined as viable cells, Annexin V-FITC+/PI− cells in Q1 as early apoptotic cells, Annexin V-FITC+/PI+ cells in Q2 as late apoptotic or secondary necrotic cells, and Annexin V-FITC−/PI+ cells in Q3 as necrotic or membrane-damaged cells. The total apoptotic population was calculated as the sum of the Q1 and Q2 populations. Unstained and single-stained controls were used to establish quadrant gates and fluorescence compensation. Both cell cycle distribution and apoptosis analyses were performed using three independent biological replicates.

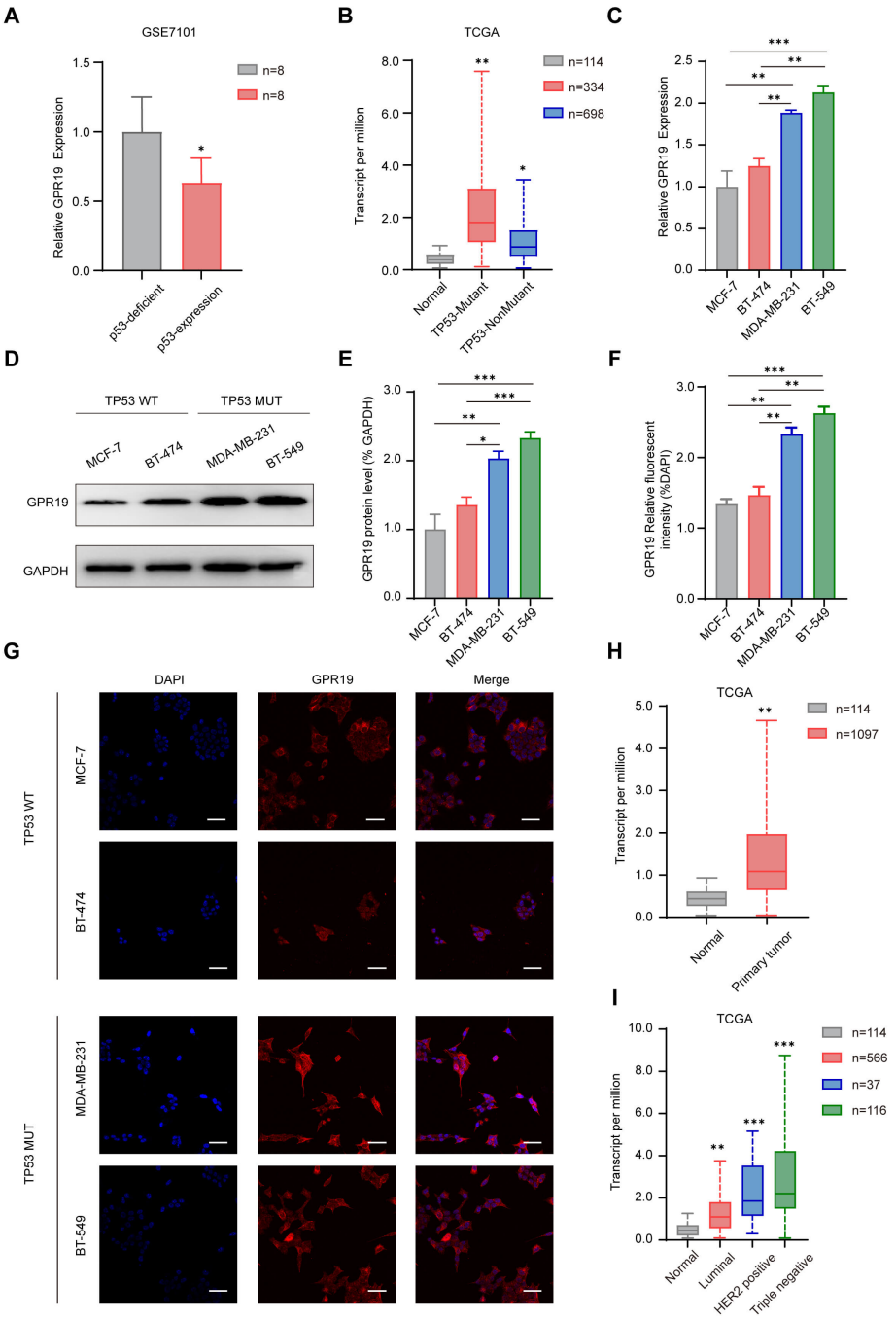

Fig. 1. GPR19 is upregulated in TP53-mutant breast cancer. (A) Analysis of the GSE7101 GEO dataset showing GPR19 mRNA expression under p53 overexpression and p53-deficient conditions. (B) TCGA-BRCA analysis of GPR19 mRNA expression according to TP53 mutational status. (C) qPCR analysis of GPR19 mRNA expression in TP53-wild-type and TP53-mutant breast cancer cell lines. (D) Representative Western blot images showing GPR19 protein expression in the indicated cell lines. (E) Densitometric quantification of GPR19 protein levels normalized to GAPDH. (F) Quantification of GPR19 fluorescence intensity in immunofluorescence assays. (G) Representative immunofluorescence images of GPR19 expression in breast cancer cells. Scale bars: 50 μm. (H) TCGA-BRCA analysis of GPR19 expression in normal and tumor tissues. (I) GPR19 expression across breast cancer molecular subtypes. Data are presented as the mean ± standard deviation. Statistical significance was determined using a two-tailed Student's *t*-test (two groups) or a one-way analysis of variance with Tukey's post hoc test (multiple groups). $*p < 0.05$, $**p < 0.01$, $***p < 0.001$. GPR19, G protein-coupled receptor 19; TP53, tumor protein p53; GEO, Gene Expression Omnibus; TCGA-BRCA, The Cancer Genome Atlas Breast Invasive Carcinoma; qPCR, quantitative polymerase chain reaction; GAPDH, glyceraldehyde-3-phosphate dehydrogenase.

2.12 RNA-Seq and Analysis

Total RNA was extracted from the indicated samples using TRIzol reagent. RNA concentration and purity were assessed using the NanoDrop 2000 spectrophotometer, and RNA integrity was evaluated using the Agilent 2100 Bioanalyzer or LabChip GX system. RNA-seq library preparation, sequencing, and primary data processing were performed by Tsingke Biotechnology Co., Ltd. RNA-seq libraries were prepared using the VAHTS Universal V6 RNA-seq Library Prep Kit for Illumina® (Vazyme, NR604-02) according to the manufacturer's instructions. Briefly, mRNA was enriched using mRNA capture beads, fragmented, reverse-transcribed into first-strand cDNA, followed by second-strand cDNA synthesis, end repair, 3′-end adenylation, adaptor ligation, fragment selection, PCR amplification, and library purification. Libraries were purified using VAHTS DNA Clean Beads (Vazyme, N411-03), quality-checked using the Qsep-400 system, and quantified using the Qubit 3.0 fluorometer with the Qubit dsDNA HS Assay Kit. Qualified libraries were sequenced on the Illumina NovaSeq 6000 platform using a paired-end 150-bp read configuration. The raw sequencing depth ranged from 19.5 to 23.7 million raw read pairs per library, corresponding to 5.9 to 7.1 Gbases per library. The raw sequencing depth for each individual library can be found in the "Availability of Data and Materials" section below. Raw reads were subjected to quality control using FastQC, followed by adapter and low-quality read trimming using fastp. Clean reads were mapped to the human reference genome GRCh38 using HISAT2 [32], and gene-level counts were obtained using featureCounts [33]. Differentially expressed genes were identified using DESeq2 [34]. p values were adjusted for multiple testing using the Benjamini–Hochberg method, and genes with an adjusted $p < 0.05$ and |log2 fold change| >1 were considered differentially expressed.

2.13 ERK Activator Treatment and Rescue Experiments

To investigate whether ERK signaling mediates the downstream effects of GPR19, cells with stable GPR19 knockdown were treated with the ERK activator Ro 67-7476 (MCE) at 10 μM for 24 h before protein extraction. Following treatment, cells were collected for analyses of p-ERK, FOXM1 expression, cell cycle distribution, apoptosis, and the expression of FOXM1 downstream G2/M regulators, including CCNB1 and PLK1. Rescue effects were compared with those of vehicle-treated control groups.

2.14 Animal Model and In Vivo Validation

Female BALB/c nude mice (4–5 weeks old) were used to establish xenograft tumors. A total of 15 mice were used and randomly allocated into three groups: shNC, shGPR19, and shGPR19 + Ro 67-7476, with five mice in each group. For tumor inoculation, 2×10^6 MDA-MB-231 cells stably expressing control shRNA or shGPR19 were suspended in 100 μL of a serum-free medium/Matrigel mixture and subcutaneously injected into the right flank of each mouse. Ro 67-7476 was administered at 4 mg/kg per injection by intraperitoneal injection three times per week. Treatment was initiated on the day of tumor cell inoculation and continued until the experimental endpoint. Tumor volumes were measured at the indicated time points and calculated using the standard formula (length × width^2)/2. At the experimental endpoint, mice were euthanized by CO_2 inhalation using a gradual displacement method, in accordance with the AVMA Guidelines for the Euthanasia of Animals. CO_2 was introduced into the chamber at a controlled rate of approximately 20–30% of the chamber volume per minute to ensure a gradual increase in CO_2 concentration and to avoid chamber pre-filling. After respiratory arrest, cervical dislocation was performed by trained personnel as a secondary physical method to confirm death. Tumors were then excised, photographed, weighed, and processed for subsequent histological and immunohistochemical analyses.

2.15 Statistical Analyses

All statistical analyses were performed using GraphPad Prism 10.0 and R (version 4.1.3). Data are presented as the mean ± standard deviation unless otherwise specified. Normality was assessed using the Shapiro–Wilk test, and homogeneity of variance was evaluated using Levene's test or Brown–Forsythe test, as appropriate. For data meeting parametric assumptions, two-group comparisons were performed using two-tailed unpaired Student's t-tests for independent samples and two-tailed paired Student's t-tests for paired tumor and adjacent non-tumorous tissue samples. Multiple-group comparisons were performed using one-way or two-way analysis of variance followed by Tukey's or Sidak's post hoc tests, as appropriate. When parametric assumptions were not met, appropriate nonparametric tests or variance-corrected tests were applied. Survival analysis was performed using the log-rank test. $p < 0.05$ was considered statistically significant. Detailed information on the commercial reagents, software, and online analysis platforms used in this study is provided in **Supplementary Table 4**.

3. Results

3.1 GPR19 Is Upregulated in TP53-Mutant Breast Cancer

As a critical tumor suppressor in breast cancer [32], the loss or mutation of TP53 drives tumor progression by enabling sustained proliferation, apoptotic evasion, and genomic instability [35]. To explore the relationship between GPR19 expression and TP53 status, we analyzed the GSE7101 GEO dataset and found that GPR19 mRNA expression was markedly reduced in the context of p53 overexpression compared with p53 deficiency (Fig. 1A) [36]. Consistently, analysis of the TCGA breast cancer cohort showed that GPR19 mRNA levels were significantly elevated in TP53-mutant tumors (Fig. 1B), suggesting that

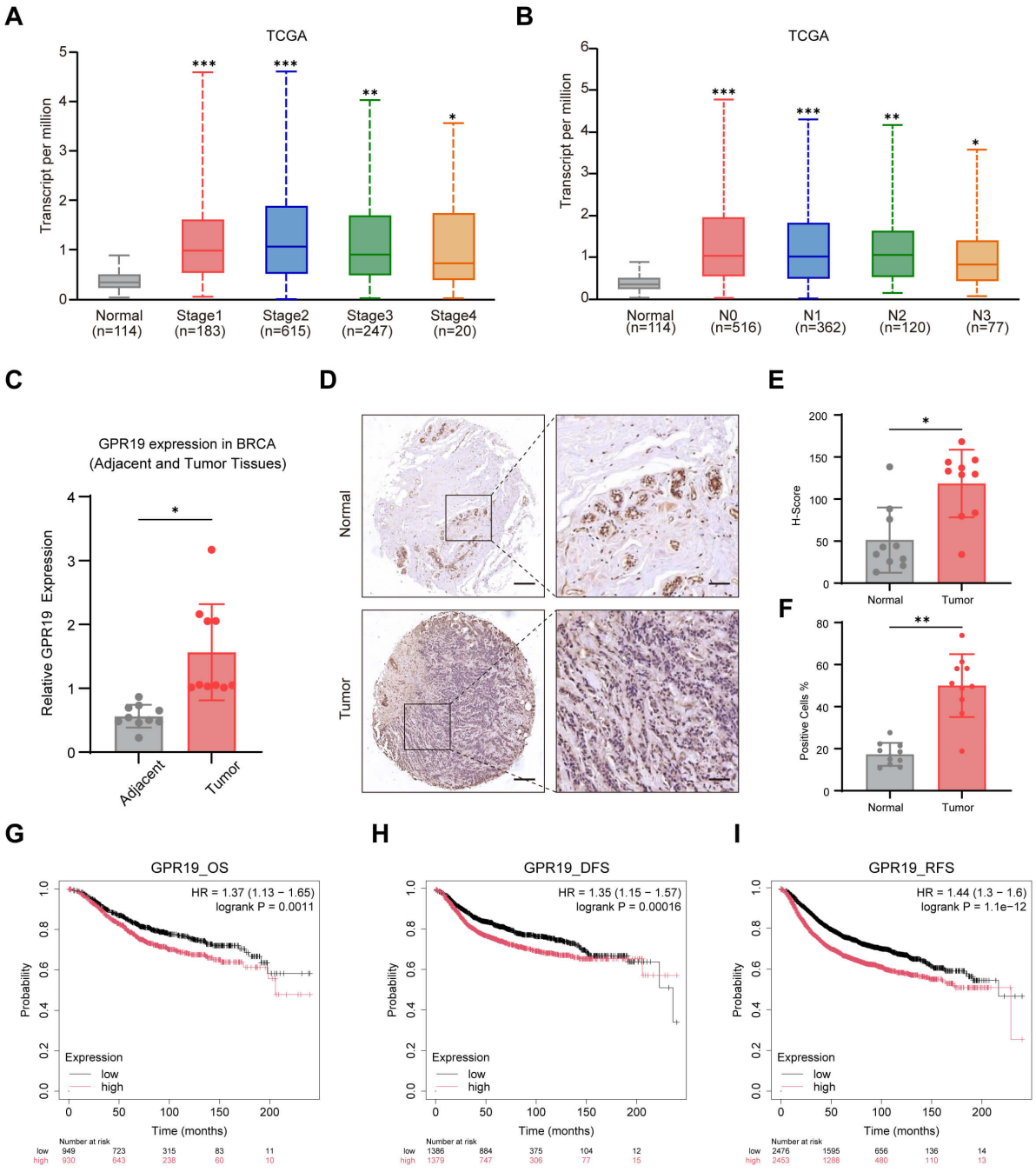

Fig. 2. Elevated GPR19 expression is associated with a poor prognosis in breast cancer. (A,B) TCGA-BRCA analysis of GPR19 expression across clinical stages and lymph node metastasis categories. (C) qPCR analysis of GPR19 mRNA expression in paired tumor and adjacent normal tissues. (D) Representative immunohistochemical staining of GPR19 in paired tissues. Scale bars: 200 μm (left) and 50 μm (right). (E,F) Quantification of H-scores and GPR19-positive cells (n = 10 paired breast tumor and adjacent normal tissue samples). (G–I) Kaplan-Meier survival curves showing OS, DFS, and RFS according to GPR19 expression using public breast cancer survival datasets. Data are presented as the mean ± standard deviation. For paired tumor and adjacent normal tissue comparisons, statistical significance was determined using two-tailed paired Student's *t*-tests or Wilcoxon matched-pairs signed-rank tests, as appropriate. For independent group comparisons, two-tailed unpaired Student's *t*-tests or one-way analysis of variance were used, as appropriate. Survival analysis was performed using the log-rank test. *$p < 0.05$, **$p < 0.01$, ***$p < 0.001$. OS, overall survival; DFS, disease-free survival; RFS, relapse-free survival.

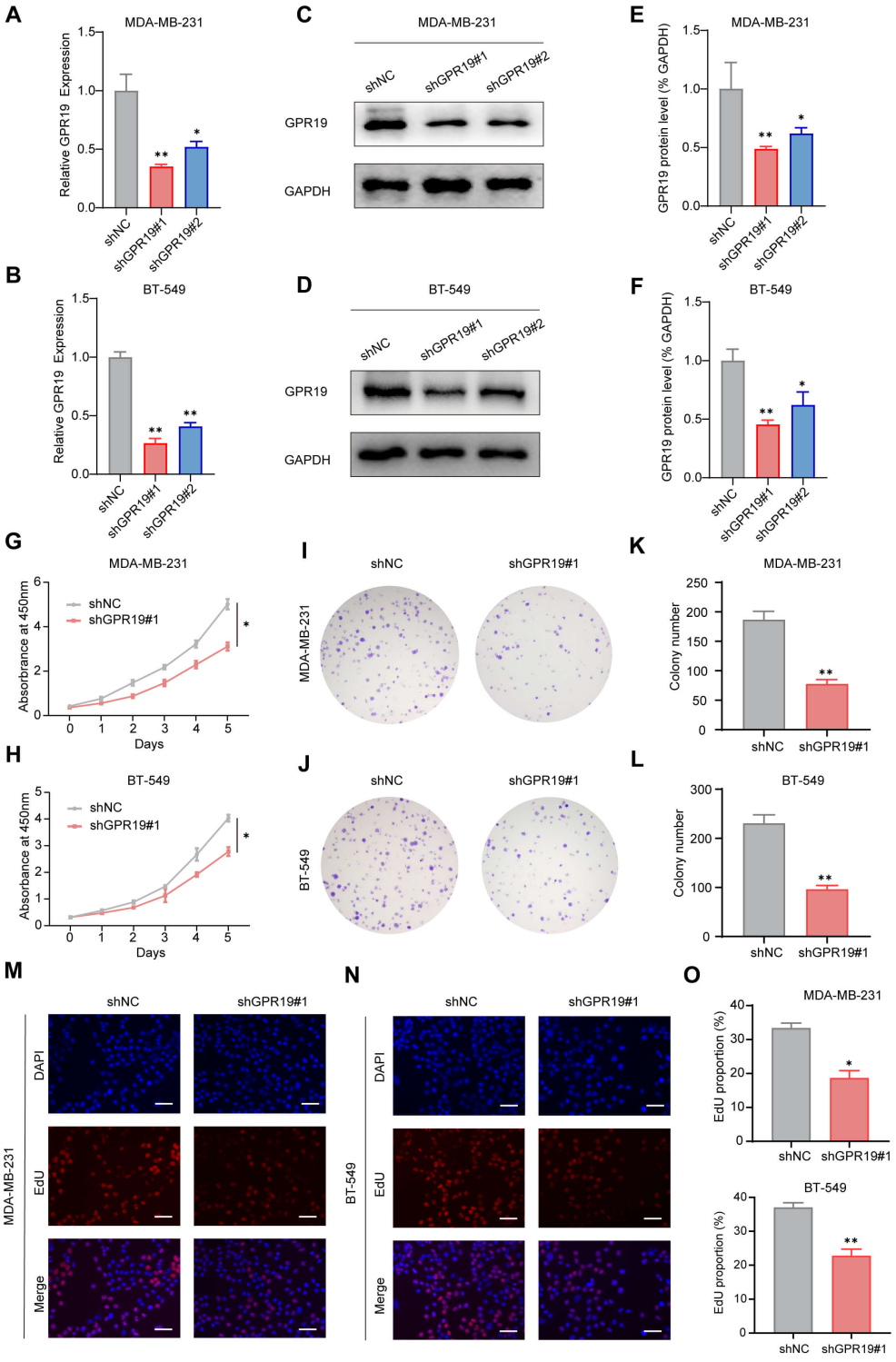

Fig. 3. GPR19 promotes proliferation of breast cancer cells. (A,B) qPCR validation of GPR19 knockdown efficiency in MDA-MB-231 and BT-549 cells. (C,D) Representative Western blot images of GPR19 protein expression. (E,F) Densitometric quantification normalized to GAPDH. (G,H) Cell proliferation assays showing cell viability over time. (I,J) Representative colony formation images. (K,L) Quantification of colony numbers. (M,N) Representative EdU staining images. Scale bars: 50 μm. (O) Quantification of EdU-positive cells. All *in vitro* experiments were independently repeated three times. Data are presented as the mean ± standard deviation. Statistical significance was determined using one-way analysis of variance with Tukey's post hoc test. *$p < 0.05$, **$p < 0.01$. EdU, 5-ethynyl-2′-deoxyuridine.

GPR19 may represent a potential malignant determinant in TP53-mutant breast cancer.

Next, we validated this expression pattern in breast cancer cell lines with distinct TP53 genotypes. qPCR analysis demonstrated that GPR19 mRNA expression was substantially higher in the TP53-mutant cell lines MDA-MB-231 and BT-549 than in the TP53-wild-type cell lines MCF-7 and BT-474 (Fig. 1C). This finding was further confirmed at the protein level by Western blotting and densitometric analyses (Fig. 1D,E). In addition, immunofluorescence staining revealed more intense GPR19 signals in TP53-mutant breast cancer cells (Fig. 1F,G).

Analysis of the TCGA dataset revealed that GPR19 is significantly upregulated in primary breast tumors compared to normal tissue, further defining its expression landscape (Fig. 1H). Stratification by molecular subtype further demonstrated that GPR19 expression was markedly enriched in TNBC compared with hormone receptor- or HER2-positive breast cancer (Fig. 1I). Collectively, these findings indicate that GPR19 is aberrantly upregulated in breast cancer, particularly in TP53-mutant and TNBC subsets.

3.2 Elevated GPR19 Predicts an Unfavorable Prognosis in Breast Cancer

Given the preferential upregulation of GPR19 in TP53-mutant breast cancer, we assessed its clinical relevance. Analysis of TCGA-BRCA RNA-seq data revealed that GPR19 expression displayed an increasing trend in advanced clinical stages and lymph node metastasis categories relative to normal breast tissues (Fig. 2A,B), suggesting a potential association with aggressive disease progression.

We further examined GPR19 expression in clinical specimens at both the mRNA and protein levels. qPCR analysis of 10 paired breast cancer and adjacent non-tumorous tissues showed that GPR19 mRNA expression was significantly elevated in tumor tissues, consistent with TCGA findings (Fig. 2C). In parallel, immunohistochemical staining of a tissue microarray containing 10 paired samples demonstrated markedly stronger GPR19 staining in tumor tissues than in matched non-tumorous controls (Fig. 2D). Quantitative immunohistochemistry assessment further confirmed that both the proportion of positive cells and H-scores were significantly increased in tumor tissues (Fig. 2E,F).

Next, we evaluated the prognostic significance of GPR19 using public breast cancer survival datasets available through the Kaplan-Meier Plotter platform. Patients with high GPR19 expression exhibited significantly worse overall survival (OS; hazard ratio [HR] = 1.37, log-rank p = 0.0011), disease-free survival (DFS; HR = 1.35, log-rank p = 0.00016), and relapse-free survival (RFS; HR = 1.44, log-rank $p = 1.1 \times 10^{-12}$) (Fig. 2G–I). Together, these multimodal patient-derived data demonstrate that GPR19 is significantly enriched in breast cancer and is closely associated with an unfavorable clinical outcome, supporting its relevance as a clinically meaningful tumor-associated protein with potential translational value.

3.3 GPR19 Drives the Malignant Proliferation of Breast Cancer Cells

To determine the functional role of GPR19 in TP53-mutant breast cancer, we established stable GPR19 knockdown models in MDA-MB-231 and BT-549 cells. qPCR analysis showed that GPR19 mRNA levels were markedly reduced in both shGPR19#1 and shGPR19#2 groups compared with the shNC group (Fig. 3A,B). Immunoblotting and densitometric quantification further confirmed efficient depletion of GPR19 at the protein level (Fig. 3C–F). Based on these validated knockdown models, a series of *in vitro* functional assays were performed to assess the effects of GPR19 on proliferative phenotypes.

Cell proliferation assays revealed that GPR19 knockdown significantly attenuated the growth curves of both cell lines, indicating reduced proliferative activity (Fig. 3G,H). Consistently, colony formation assays showed that GPR19 depletion markedly reduced the number of colonies formed by MDA-MB-231 and BT-549 cells, suggesting compromised long-term proliferative and clonogenic potential (Fig. 3I–L). Moreover, EdU incorporation assays demonstrated a pronounced decrease in the proportion of EdU-positive cells upon GPR19 knockdown, indicating impaired DNA synthesis and replicative activity (Fig. 3M–O).

Taken together, these findings demonstrate that GPR19 depletion suppresses multiple dimensions of the proliferative phenotype in TP53-mutant breast cancer cells, including cell viability, clonogenic expansion, and DNA synthesis, supporting a robust pro-proliferative role for GPR19 in breast cancer.

3.4 GPR19 Depletion Induces G2/M Arrest and Apoptosis in Breast Cancer Cells

To investigate the mechanisms underlying the pro-proliferative effect of GPR19, we analyzed its relationship with cell cycle-related pathways. Correlation analyses showed that GPR19 expression was significantly positively associated with both the G2/M checkpoint signature and proliferation-related scores (Fig. 4A,B). Hallmark enrichment analysis further demonstrated that GPR19-associated genes were predominantly enriched in cell cycle-related pathways, including G2/M checkpoint and E2F targets (Fig. 4C), implicating GPR19 in mitotic control.

We assessed the effect of GPR19 depletion on cell cycle distribution by flow cytometry. In both MDA-MB-231 and BT-549 cells, GPR19 knockdown reduced the proportion of cells in G1 phase while increasing the fractions in S and G2/M phases, with a prominent accumulation at G2/M (Fig. 4D–G). These findings indicate abnormal cell cycle progression and indicate that GPR19 deficiency hinders proper transition through the G2/M checkpoint.

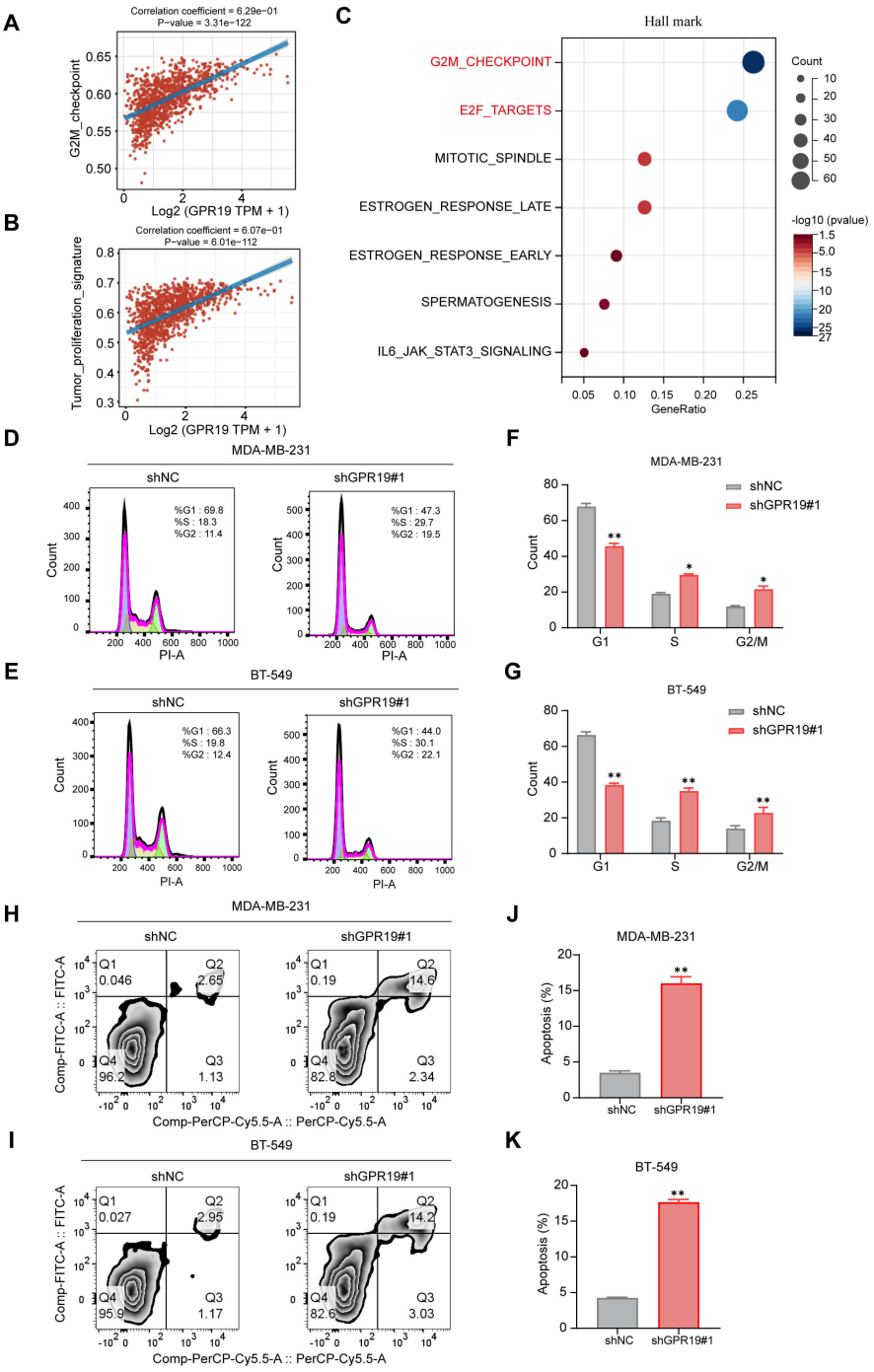

Fig. 4. GPR19 depletion induces G2/M arrest and apoptosis. (A,B) Correlation analyses between GPR19 expression and the G2/M checkpoint signature or proliferation-related scores in breast cancer datasets. (C) Hallmark enrichment analysis of GPR19-associated genes, highlighting enrichment of cell cycle-related pathways, including G2/M checkpoint, and E2F targets. (D,E) Representative flow cytometry plots showing cell cycle distribution in MDA-MB-231 and BT-549 cells following GPR19 knockdown. (F,G) Quantification of the percentages of cells in G1, S, and G2/M phases in the indicated groups. (H,I) Representative Annexin V/PI apoptosis plots in control and GPR19-knockdown cells. (J,K) Quantification of apoptotic cell fractions. Flow cytometry experiments for cell cycle and apoptosis analyses were independently repeated three times. Data are presented as the mean ± standard deviation. Statistical significance was determined using one-way analysis of variance. *$p < 0.05$, **$p < 0.01$. PI, propidium iodide.

In parallel, Annexin V/PI assays showed that GPR19 knockdown significantly increased the apoptotic fraction in both breast cancer cell lines (Fig. 4H–K). Collectively, these results suggest that GPR19 promotes the malignant

proliferation of breast cancer cells, at least in part, by sustaining G2/M checkpoint-associated cell cycle progression while inhibiting apoptosis.

3.5 GPR19 Sustains Cell Cycle Progression by Activating the ERK–FOXM1 Axis

To further delineate the molecular mechanism by which GPR19 regulates cell cycle progression in breast cancer cells, we examined GPR19-associated transcriptional features and downstream signaling pathways. RNA-seq analysis comparing shGPR19 and shNC cells revealed 159 upregulated and 377 downregulated genes among 18,011 analyzed genes, with 17,475 genes classified as unchanged. Among these, FOXM1 was identified as a key downregulated cell cycle-related gene after GPR19 knockdown (Fig. 5A). Given the established role of FOXM1 as a central regulator of G2/M progression, we further examined the relationship between GPR19 and FOXM1 expression in breast cancer. Correlation analysis demonstrated a significant positive association between GPR19 and FOXM1 expression (Fig. 5B), which was further validated in the TCGA dataset (**Supplementary Fig. 1A**). Functional enrichment analysis of the RNA-seq data revealed that GPR19-downregulated genes were primarily clustered in cell cycle regulatory processes, including positive regulation of the cell cycle, positive regulation of the cell cycle checkpoint, and regulation of the mitotic spindle checkpoint (Fig. 5C). In parallel, FOXM1 expression was positively correlated with both the G2/M checkpoint signature and proliferation-related scores (**Supplementary Fig. 1B,C**), suggesting that GPR19 may contribute to cell cycle maintenance through FOXM1.

Following GPR19 knockdown in MDA-MB-231 and BT-549 cells, both the mRNA and protein levels of FOXM1 were markedly reduced, accompanied by a substantial decrease in p-ERK1/2 levels, whereas total ERK1/2 expression remained largely unchanged (Fig. 5D,E; **Supplementary Fig. 1D,E**). Given the established role of ERK phosphorylation in FOXM1 activation [37], we hypothesized that GPR19 regulates FOXM1 by modulating ERK phosphorylation rather than its overall abundance. Importantly, treatment with the ERK activator Ro 67-7476 partially restored FOXM1 expression (Fig. 5D,E; **Supplementary Fig. 1D,E**), suggesting that the downregulation of FOXM1 is, at least in part, dependent on impaired ERK activity.

Functionally, flow cytometry showed that Ro 67-7476 partially corrected cell cycle disruption induced by GPR19 depletion (Fig. 5F,G). In parallel, ERK activation also reduced the level of apoptosis induced by GPR19 deficiency (Fig. 5H,I), further supporting a critical role for ERK signaling in mediating the survival-promoting function of GPR19.

We next examined key FOXM1 downstream effectors involved in G2/M progression. CCNB1 and PLK1 were markedly downregulated upon GPR19 knockdown and were partially restored following ERK activation (Fig. 5J,K). Previous FOXM1 chromatin immunoprecipitation (ChIP) and ChIP-seq studies identified CCNB1 and PLK1 as promoter-associated FOXM1-bound cell cycle genes, supporting their classification as canonical FOXM1 transcriptional targets [38]. Concurrently, GSEA of FOXM1-silenced MDA-MB-231 cells revealed significant negative enrichment of the HALLMARK_G2M_CHECKPOINT pathway and significant positive enrichment of the HALLMARK_APOPTOSIS pathway (**Supplementary Fig. 1F,G**). These findings indicate that inhibiting FOXM1 suppresses G2/M cell cycle progression while increasing apoptosis. These findings indicate that GPR19 drives breast cancer cell cycle progression and inhibits apoptosis by increasing ERK phosphorylation, which sustains FOXM1 expression and activates the FOXM1-associated G2/M transcriptional program (specifically CCNB1 and PLK1). However, the direct occupancy of FOXM1 at these sites in the absence of GPR19 requires further validation.

3.6 FOXM1 Is Overexpressed in Breast Cancer and Indicates a Poor Prognosis

Given the central role of FOXM1 in the GPR19–ERK–FOXM1 signaling axis, we next explored its clinical significance in breast cancer. In the BRCA cohort, FOXM1 expression was significantly positively correlated with both CCNB1 and PLK1 (Fig. 6A,B). This association became even more evident when FOXM1 was evaluated against a cell cycle-related gene set composed of CCNB1 and PLK1 (Fig. 6C), further supporting a close relationship between FOXM1 and cell cycle progression in breast cancer.

Next, we characterized the expression profile of FOXM1 in public breast cancer datasets. TCGA-BRCA analysis showed that FOXM1 expression was significantly elevated in TP53-mutant breast cancers relative to both normal breast tissues and TP53-non-mutant tumors (Fig. 6D). FOXM1 expression was also markedly higher in primary breast tumors than in normal breast tissues (Fig. 6E). Stratification by molecular subtype further revealed that FOXM1 was upregulated across all major breast cancer subtypes, with the highest expression observed in TNBC (Fig. 6F). These findings suggest that FOXM1 overexpression is a common feature of breast cancer and may be particularly associated with more aggressive molecular subtypes.

To further assess its relevance to disease progression, we analyzed FOXM1 expression across clinical stages and lymph node metastasis categories. FOXM1 expression was significantly elevated in stage I–IV breast cancers compared with normal tissues (Fig. 6G), indicating that its upregulation is maintained throughout disease progression. Similarly, FOXM1 expression was significantly increased across all lymph node categories, including N0, N1, N2, and N3, relative to normal breast tissues (Fig. 6H), mirroring the expression pattern observed for GPR19.

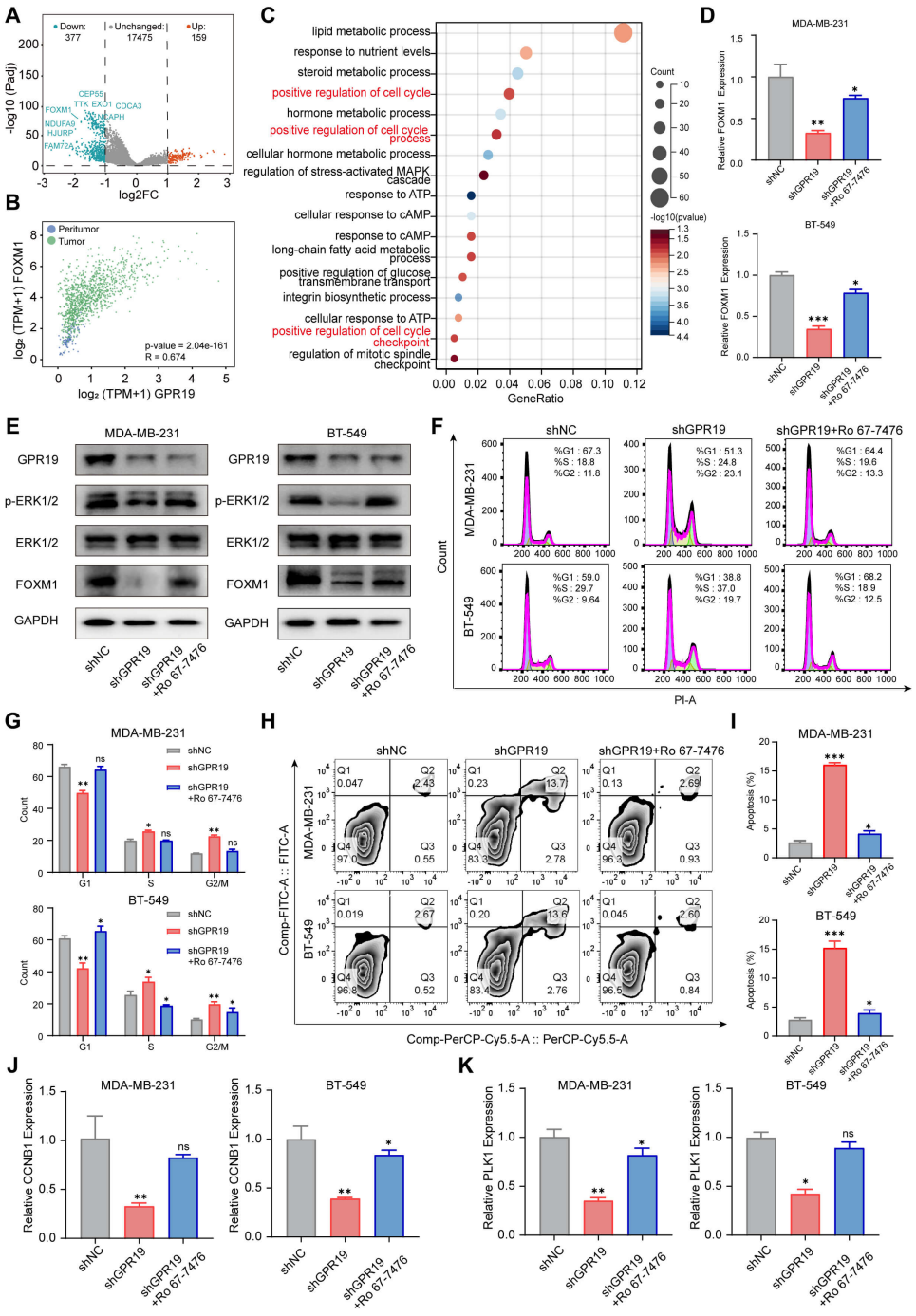

Fig. 5. GPR19 sustains cell cycle progression by activating the ERK–FOXM1 axis. (A) Volcano plot showing differentially expressed genes in shGPR19 cells compared with shNC cells based on RNA-seq analysis. FOXM1 is highlighted as a representative downregulated gene after GPR19 knockdown. (B) Correlation analysis between GPR19 and FOXM1 expression in breast cancer. (C) Functional enrichment analysis of RNA-seq data showing that GPR19-related genes are enriched in cell cycle regulatory processes, including the cell cycle-related biological processes highlighted in red. (D,E) qPCR and Western blot analyses of FOXM1 and ERK signaling in GPR19-knockdown cells with or without Ro 67-7476 treatment. (F,G) Flow cytometry analysis of cell cycle distribution in the indicated groups. (H,I) Annexin V/PI assays showing apoptosis in the indicated groups. (J,K) qPCR analyses of the FOXM1 downstream G2/M regulators CCNB1 and PLK1. All rescue experiments were independently repeated three times. Data are presented as the mean ± standard deviation. Statistical significance was determined as described in the Methods. ns, not significant; *$p < 0.05$, **$p < 0.01$, ***$p < 0.001$. ERK, extracellular signal-regulated kinase; FOXM1, forkhead box protein M1; shGPR19, short hairpin RNA targeting G protein-coupled receptor 19; shNC, short hairpin RNA negative control; RNA-seq, RNA sequencing; CCNB1, cyclin B1; PLK1, polo-like kinase 1.

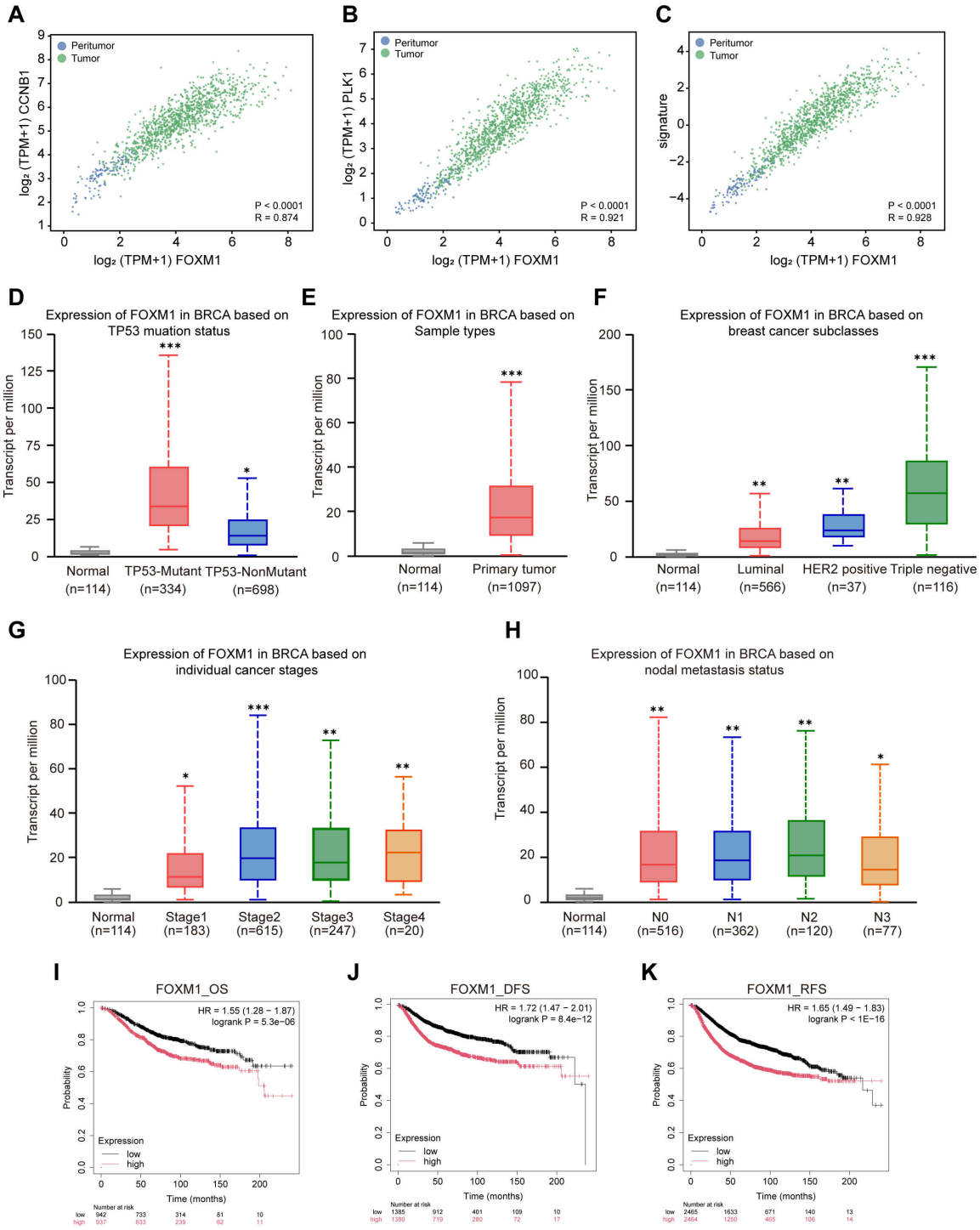

Fig. 6. FOXM1 is overexpressed in breast cancer and indicates a poor prognosis. (A,B) Correlation analyses between FOXM1 and CCNB1 or PLK1 expression in the BRCA cohort. (C) Correlation analysis between FOXM1 expression and a cell cycle-related gene set composed of CCNB1 and PLK1. (D) TCGA-BRCA analysis of FOXM1 expression according to TP53 mutational status. (E) FOXM1 expression in normal breast tissues and primary breast tumors. (F) FOXM1 expression across breast cancer molecular subtypes. (G,H) FOXM1 expression across clinical stage and lymph node metastasis categories. (I–K) Kaplan-Meier survival analyses of OS, DFS, and RFS according to FOXM1 expression. Data are presented as the mean ± standard deviation. Statistical significance was determined as described in the Methods. *$p < 0.05$, **$p < 0.01$, ***$p < 0.001$.

Finally, Kaplan-Meier survival analyses demonstrated that high FOXM1 expression was significantly associated with shorter OS, distant metastasis-free survival, and RFS (Fig. 6I–K). Together, these findings identify FOXM1 as a clinically relevant oncogenic factor in breast cancer that is closely associated with aggressive progression and adverse patient outcomes.

3.7 GPR19–ERK–FOXM1 Axis Is Functionally Validated In Vivo

To confirm that the GPR19–ERK–FOXM1 axis drives tumor growth *in vivo*, we established a subcutaneous xenograft model in nude mice using MDA-MB-231 cells and assigned the animals to the shNC, shGPR19, and shGPR19 + Ro 67-7476 groups (Fig. 7A). Compared with the shNC group, GPR19 knockdown markedly suppressed xenograft growth, as evidenced by reduced tumor volume and significantly lower tumor weight at the experimental endpoint. Notably, treatment with Ro 67-7476 partially reversed the growth-inhibitory phenotype induced by GPR19 silencing (Fig. 7B,C).

Following GPR19 knockdown, hematoxylin and eosin staining showed greater intratumoral necrosis, which was mitigated by activating ERK (Fig. 7D). Immunohistochemical analysis of Ki-67 showed that GPR19 knockdown significantly reduced tumor cell proliferation, while treatment with Ro 67-7476 partially rescued this effect (Fig. 7E). Conversely, TUNEL staining revealed increased apoptotic activity in the shGPR19 group, which was partially attenuated following rescue treatment (Fig. 7F). These findings indicate that GPR19 depletion suppresses tumor growth *in vivo* by concurrently impairing proliferation and enhancing apoptosis.

We next performed immunohistochemical analyses of xenograft tissues to further characterize the status of the GPR19–ERK–FOXM1 signaling cascade (Fig. 7G). As expected, GPR19 expression was markedly reduced in the shGPR19 group (Fig. 7H). Total ERK levels remained largely unchanged among the three groups, whereas p-ERK levels were substantially decreased following GPR19 knockdown and were partially restored after Ro 67-7476 administration (Fig. 7I,J). Consistently, FOXM1 expression was significantly downregulated in the shGPR19 group and was partially restored after pharmacological ERK activation with Ro 67-7476 (Fig. 7K). In line with these findings, expression of the FOXM1 downstream G2/M regulators CCNB1 and PLK1 was also markedly reduced in the shGPR19 group and partially restored upon rescue treatment (Fig. 7L–N). Taken together, these *in vivo* data indicate that GPR19 knockdown markedly suppresses xenograft growth and regulates the expression of FOXM1 and its downstream effectors, CCNB1 and PLK1, by modulating ERK phosphorylation.

4. Discussion

GPCR signaling is now recognized as a highly dynamic and druggable oncogenic network in cancer biology [39]. Abnormal GPCR activation in cancer is driven by more than just receptor overexpression, ligand enrichment, and the tumor microenvironment. It also results from biased G protein signaling, β-arrestin-dependent pathways, receptor transactivation, and intracellular signal recycling [40]. Through these mechanisms, GPCRs sustain and amplify multiple oncogenic pathways, including MAPK/ERK, phosphoinositide 3-kinase/AKT/mammalian target of rapamycin, Rho GTPases, Janus kinase/signal transducer and activator of transcription, and Yes-associated protein/transcriptional coactivator with PDZ-binding motif, thereby driving a broad spectrum of malignant phenotypes [11,41]. Emerging evidence redefines GPCRs beyond traditional membrane receptors, highlighting their role as central signaling hubs. They connect internal tumor programs with the microenvironment to drive proliferation, metastasis, metabolic reprogramming, immune evasion, and drug resistance [42].

Current literature on GPR19 in cancer is scarce, and its biological role appears to be highly context-dependent [43]. While initial research linked GPR19 to G2/M progression in lung cancer and E-cadherin-related plasticity in breast cancer, more recent reports have suggested a wider role in metabolic stress responses and biomarker profiles across melanoma and other malignancies [44]. A significant, unresolved issue is that GPR19 remains a poorly characterized Class A orphan GPCR, lacking a universally accepted endogenous ligand [45]. Although adropin has been proposed as a potential ligand for GPR19 and reportedly activates MAPK/ERK signaling in breast cancer cells, this ligand–receptor relationship remains insufficient to fully define the upstream activation mechanism of GPR19 in cancer contexts [19,46]. In addition, the G-protein coupling subtype of GPR19 has not been fully characterized. While GPR19 is likely associated with Gαi signaling, definitive experimental evidence identifying its specific Gα subunit coupling in breast cancer cells remains limited.

Given this context, our findings reveal a key mechanism: GPR19 drives breast cancer proliferation by activating the ERK–FOXM1 pathway and its downstream cell cycle targets. Therefore, GPR19 may serve as an active upstream regulator of mitotic competence in breast cancer cells, rather than simply marking the tumor state. This interpretation is consistent with the growing consensus that, despite limited characterization, orphan GPCRs exert substantial control over malignant phenotypes by integrating signaling and metabolic pathways [47,48]. At the same time, it is crucial to emphasize that GPR19 is context-dependent, with its downstream signaling varying based on tumor type and cellular state.

Our findings provide a new mechanistic explanation for the current understanding of TP53-altered breast can-

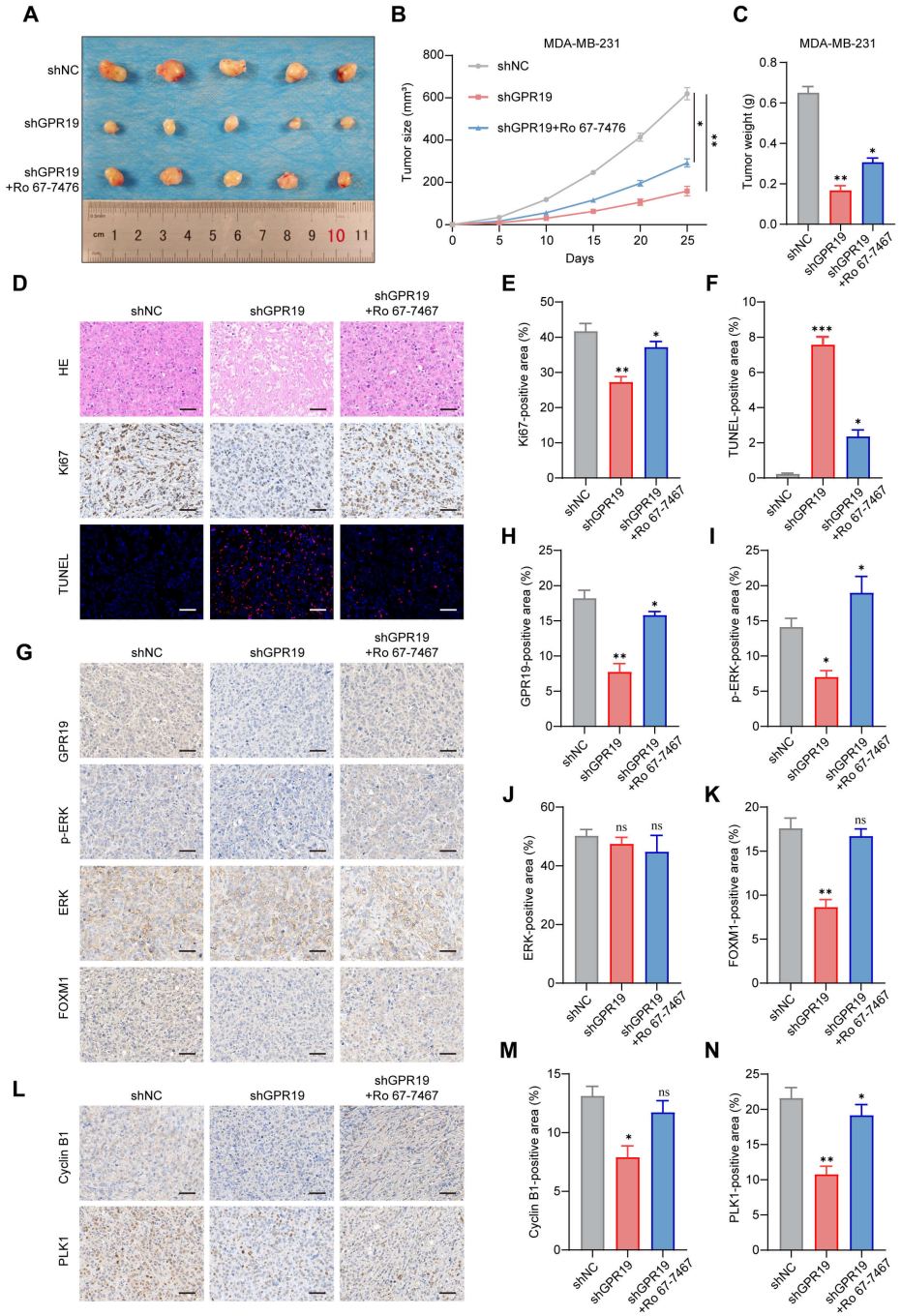

Fig. 7. The GPR19-ERK-FOXM1 axis is functionally validated *in vivo*. (A) Representative images of tumors harvested from the shNC, shGPR19, and shGPR19 + Ro 67-7476 groups. Each group included five mice (n = 5 per group). (B,C) Tumor growth curves and tumor weights at the experimental endpoint of xenografts in the indicated groups. (D) Hematoxylin and eosin staining, Ki-67 immunohistochemical staining, and TUNEL staining were performed to assess histopathological alterations, proliferative activity, and apoptotic cell proportion, respectively. Scale bars: 50 μm. (E,F) Quantification of Ki-67 and TUNEL staining in different treatment groups. (G) Representative immunohistochemical staining of the GPR19–ERK–FOXM1 axis in xenograft tissues. Scale bars: 50 μm. (H–K) Quantification of the staining intensity of the GPR19–ERK–FOXM1 axis. (L) Representative immunohistochemical staining of CCNB1 and PLK1 in xenograft tissues. Scale bars: 50 μm. (M,N) Quantification of the staining intensity of CCNB1 and PLK1. Data are presented as the mean ± standard deviation. Statistical significance was determined as described in the Methods. ns, not significant; *$p < 0.05$, **$p < 0.01$, ***$p < 0.001$. TUNEL, terminal deoxynucleotidyl transferase-mediated dUTP nick-end labeling.

cer. Long recognized as a driver of aggressive cancer, the TP53 mutation is now understood to act beyond a mere loss of function by inducing genomic instability, context-dependent gain-of-function properties, and altered therapeutic vulnerabilities [49,50,51]. Within this context, our finding that GPR19 is preferentially upregulated in TP53-mutant breast cancer is of particular significance. Both bioinformatics analyses and experimental validation consistently demonstrated that GPR19 expression was significantly higher in TP53-mutant cells than in TP53 wild-type cells. Moreover, GPR19 enrichment in TNBC correlated with a poor prognosis, suggesting that it is likely more than a coincidental finding and may instead be functionally linked to the malignant molecular features associated with TP53 deficiency.

Functionally, our study demonstrates that GPR19 exerts a marked pro-proliferative effect on TP53-mutant breast cancer cells by coordinating both cell cycle progression and cell survival. Silencing GPR19 significantly suppressed cell proliferation, colony formation, and DNA synthesis in MDA-MB-231 and BT-549 cells, accompanied by G2/M arrest, a reduction in the G1 phase cell population, and increased apoptosis. These findings indicate that GPR19 sustains the aggressive phenotype of TP53-mutant breast cancer cells by driving malignant proliferation and inhibiting apoptosis. Public ChIP-Atlas data further suggest potential p53 occupancy at the GPR19 locus. The higher number of p53 binding peaks in MDA-MB-231 compared to MCF-7 cells highlights that p53 occupancy in this genomic region may be cell context-dependent. These results are consistent with our observation of higher GPR19 expression in TP53-mutant versus TP53-wild-type breast cancer cells.

This study identifies the ERK–FOXM1 axis as the primary mechanism through which GPR19 drives breast cancer cell cycle progression [50]. ERK signaling, an established oncogenic pathway, integrates receptor tyrosine kinase and GPCR signals to promote cell cycle progression, DNA damage repair, and therapeutic tolerance [52,53,54]. Mechanistically, ERK signaling may regulate FOXM1 through several complementary mechanisms. Previous studies have shown that aberrant ERK activation can increase FOXM1 expression and contribute to FOXM1-dependent malignant phenotypes [55], while FOXM1 activity is also influenced by phosphorylation-dependent regulation [56]. In particular, MAPK/ERK signaling reportedly promotes FOXM1 activation by enhancing its transcriptional activity and nuclear function, thereby facilitating the expression of cell cycle genes required for G2/M progression [57,58].

FOXM1 is frequently overexpressed in TNBC and has been consistently linked to poor prognosis, enhanced proliferation, migration, invasion, and therapeutic resistance [59], a pattern that closely parallels the expression profile of GPR19 in breast cancer. One of the most prominent functions of FOXM1 is the maintenance of cell cycle programs [60], as it drives G1/S and G2/M transitions through transcriptional activation of genes involved in cell division, including CCNB1 and PLK1 [61,62]. Importantly, the oncogenic role of FOXM1 is particularly critical in the absence of functional p53. While wild-type p53 suppresses excessive proliferation and regulates the cell cycle control, TP53 mutation or loss removes this restriction, allowing unchecked FOXM1-dependent transcriptional activity [63]. As a major regulator of G2/M progression, FOXM1 may serve as an important effector of TP53-deficient malignant proliferation.

Consistent with these concepts, our RNA-seq and correlation analyses consistently identified FOXM1 as a GPR19-associated gene, and GPR19 depletion markedly reduced FOXM1 expression at both the mRNA and protein levels. Notably, this reduction was accompanied by a pronounced decrease in ERK phosphorylation, whereas total ERK expression remained largely unchanged, indicating that GPR19 primarily regulates signaling activity rather than ERK abundance. Further mechanistic support for this model was provided by rescue experiments using the ERK activator Ro 67-7476. Pharmacological ERK activation partially restored FOXM1 expression in GPR19-deficient cells and alleviated the associated cell cycle disruption and apoptosis. In addition, expression of the FOXM1 downstream G2/M regulators CCNB1 and PLK1, which was markedly reduced following GPR19 knockdown, was partially recovered upon ERK activation. Together, these findings support the notion that GPR19 acts upstream of ERK and FOXM1 and sustains proliferative signaling in breast cancer cells through the canonical FOXM1 transcriptional targets CCNB1 and PLK1.

The functional importance of this signaling cascade was further confirmed *in vivo*. In xenograft models, GPR19 knockdown significantly suppressed tumor growth, reduced tumor weight, decreased Ki-67 staining, and increased TUNEL positivity, indicating that loss of GPR19 inhibits tumor proliferation while promoting apoptosis *in vivo*. Notably, pharmacological ERK activation with Ro 67-7476 partially reversed these phenotypes and restored the expression of FOXM1, CCNB1, and PLK1 in the GPR19-knockdown background, supporting ERK signaling as a downstream mediator of GPR19-associated effects. The strong concordance between *in vitro* and *in vivo* findings provides compelling evidence for the validity of the proposed GPR19–ERK–FOXM1 signaling model.

In summary, this study establishes GPR19 as a key oncogenic driver and valuable clinical biomarker for breast cancer, particularly within the TP53-mutant and TNBC subtypes. GPR19 drives malignant progression by activating the ERK/FOXM1 signaling axis to sustain G2/M regulators (CCNB1 and PLK1), accelerating the cell cycle progression, and inhibiting apoptosis. These results identify the GPR19–ERK–FOXM1 axis as a key regulator of ag-

gressive breast cancer and support future investigation into GPR19-targeted therapeutic strategies.

5. Limitations

One limitation of this study is that the regulatory relationship between p53 and GPR19 was not directly validated at the variant level. While ChIP-Atlas data indicate p53 binds to the GPR19 locus, these findings do not confirm whether this interaction drives functional transcriptional regulation. Moreover, TP53-mutant status should be interpreted cautiously because TCGA tumors contain heterogeneous TP53 variants, whereas the cell lines used in this study harbor defined TP53 backgrounds, including TP53 R280K in MDA-MB-231, TP53 R249S in BT-549, and wild-type TP53 in MCF-7 and BT-474 [64,65]. Consequently, this study cannot determine if the observed GPR19-associated phenotypes results from the loss of wild-type p53 function, a gain-of-function by mutant p53, or a combination of both. In addition, the functional requirement of FOXM1 in the GPR19-dependent phenotype was not directly examined. Although ERK activation with Ro 67-7476 partially restored FOXM1 expression and alleviated the cell cycle arrest and apoptosis induced by GPR19 depletion, these findings do not establish whether FOXM1 is necessary for the biological effects of GPR19. Future studies using isogenic TP53-edited models, ChIP-qPCR, promoter–reporter assays, FOXM1 knockdown, FOXM1 rescue, and epistasis experiments in GPR19-manipulated cells are required to clarify variant-specific p53 regulation of GPR19 and determine whether FOXM1 acts as an essential downstream effector of the GPR19–ERK signaling axis.

6. Conclusions

This study systematically elucidates the oncogenic role and clinical significance of GPR19 in breast cancer, providing a novel perspective for understanding the progression of TP53-mutant breast cancer. Mechanistically, we demonstrate for the first time that GPR19 drives breast cancer progression through the ERK–FOXM1 signaling axis by: (1) sustaining G2/M cell cycle progression by enhancing ERK phosphorylation and maintaining the expression of FOXM1 and its downstream effectors CCNB1 and PLK1, thereby promoting malignant proliferation; and (2) suppressing apoptosis, which together support tumor growth both *in vitro* and *in vivo*. Rescue experiments using the ERK activator Ro 67-7476 further validate that ERK signaling is a critical mediator of GPR19-dependent oncogenic effects, supporting GPR19 as a potential upstream therapeutic target. Although the precise molecular basis by which GPR19 activates ERK remains to be further clarified, this work provides a new rationale for prognostic stratification and targeted intervention in aggressive breast cancer, particularly in TP53-mutant subsets, and lays the foundation for future translational and preclinical studies.

Abbreviations

BRCA, breast invasive carcinoma; CCNB1, cyclin B1; DFS, disease-free survival; ERK, extracellular signal-regulated kinase; FOXM1, forkhead box M1; GEO, Gene Expression Omnibus; GEPIA3, Gene Expression Profiling Interactive Analysis 3; GPCR, G protein-coupled receptor; GPR19, G protein-coupled receptor 19; HER2, human epidermal growth factor receptor 2; OS, overall survival; PI, propidium iodide; PLK1, polo-like kinase 1; RFS, relapse-free survival; RNA-seq, RNA sequencing; TCGA, The Cancer Genome Atlas; TNBC, triple-negative breast cancer; TUNEL, terminal deoxynucleotidyl transferase dUTP nick end labeling.

Availability of Data and Materials

The raw RNA-seq FASTQ files generated in this study have been deposited in the NCBI Sequence Read Archive under BioProject accession number PRJNA1474259, and the detailed sample-to-condition information is provided in **Supplementary Table 5**. Other data supporting the findings of this study are available from the corresponding authors upon reasonable request.

Author Contributions

Conceptualization, JQ, HY and SL; Data curation, HL and SG; Formal analysis, CT, LT and YP; Funding acquisition, HY and SL; Investigation, KL, KH, HL and YP; Methodology JQ and LT; Project administration, SL; Resources, YL and LT; Supervision, HY and SL; Validation, HL, QL and CY; Writing–original draft, JQ, CT and HL; Writing–review and editing, CT and YP. All authors have read and agreed to the final version of the manuscript. All authors contributed to editorial changes in the manuscript. All authors have participated sufficiently in the work and agreed to be accountable for all aspects of the work.

Ethics Approval and Consent to Participate

Matched clinical breast tumor tissues and adjacent normal tissues were obtained from breast cancer patients undergoing surgical resection at the First Affiliated Hospital of Chongqing Medical University for tissue microarray construction and IHC analyses. Written informed consent was obtained from all participants prior to sample collection and all procedures were conducted in strict accordance with the Declaration of Helsinki. Sample collection and use were approved by the Ethics Committee of the First Affiliated Hospital of Chongqing Medical University (Approval No. K2023-513). The animal experiments were approved by the Medical Research Ethics Committee of the First Affiliated Hospital of Chongqing Medical University (Approval No. IACUC-CQMU-2025-10026) and were conducted in accordance with institutional guidelines, the Regulations for the Administration of Affairs Concerning Experimental Animals (2017 revision), and the Laboratory

Animal—Guideline for Ethical Review of Animal Welfare (GB/T 35892-2018). This study is reported in compliance with the ARRIVE guidelines.

Acknowledgment

We would like to express our sincere gratitude to Professor Wang Wang for her assistance with the statistical analysis of the experimental data. The graphical abstract was created with BioRender.

Funding

This project was financially supported by the following: 1. Postdoctoral Science Foundation of Chongqing (Grant No. CSTB2023NSCQ-BHX0023). 2. The National Natural Science Foundation of China (NSFC, 82503580). 3. The National Natural Science Foundation of China (NSFC, 82573678). 4. The Chongqing Medical Scientific Research Project (Joint Project of Chongqing Health Commission and Science and Technology Bureau, 2025DBXM005). 5. The Graduate Supervisor Team Development Program; the First Affiliated Hospital of Chongqing Medical University (CYYY-DSTDXM202502).

Conflicts of Interest

The authors declare no conflicts of interest.

Declaration of AI and AI-Assisted Technologies in the Writing Process

During the preparation of this manuscript, the authors used ChatGPT by OpenAI only to assist with English language polishing and grammar checking. All scientific content, including the study design, experimental data, data analysis, interpretation of results, and conclusions, was developed and verified by the authors. The authors carefully reviewed and edited the AI-assisted output and take full responsibility for the entire content of the manuscript.

Supplementary Material

Supplementary material associated with this article can be found, in the online version, at https://doi.org/10.31083/FBL52064.

References

[1] Sung H, Ferlay J, Siegel RL, Laversanne M, Soerjomataram I, Jemal A, et al. Global Cancer Statistics 2020: GLOBOCAN Estimates of Incidence and Mortality Worldwide for 36 Cancers in 185 Countries. CA: a Cancer Journal for Clinicians. 2021; 71: 209–249. https://doi.org/10.3322/caac.21660

[2] Guo L, Kong D, Liu J, Zhan L, Luo L, Zheng W, et al. Breast cancer heterogeneity and its implication in personalized precision therapy. Experimental Hematology & Oncology. 2023; 12: 3. https://doi.org/10.1186/s40164-022-00363-1

[3] Xiong X, Zheng LW, Ding Y, Chen YF, Cai YW, Wang LP, et al. Breast cancer: pathogenesis and treatments. Signal Transduction and Targeted Therapy. 2025; 10: 49. https://doi.org/10.1038/s41392-024-02108-4

[4] Okines A, Turner N. Developing therapies for triple-negative breast cancer subtypes. The Lancet. Oncology. 2024; 25: 149–151. https://doi.org/10.1016/S1470-2045(23)00639-3

[5] Li W, Li L, Yang H, Shi C, Lei Z, Guo L, et al. Unraveling the Role of *TP53* in Colorectal Cancer Therapy: From Wild-Type Regulation to Mutant. Frontiers in Bioscience (Landmark Edition). 2024; 29: 272. https://doi.org/10.31083/j.fbl2907272

[6] Joerger AC, Stiewe T, Soussi T. TP53: the unluckiest of genes? Cell Death and Differentiation. 2025; 32: 219–224. https://doi.org/10.1038/s41418-024-01391-6

[7] Zhang H, Xu J, Long Y, Maimaitijiang A, Su Z, Li W, et al. Unraveling the Guardian: p53's Multifaceted Role in the DNA Damage Response and Tumor Treatment Strategies. International Journal of Molecular Sciences. 2024; 25: 12928. https://doi.org/10.3390/ijms252312928

[8] Janic A, Abad E, Amelio I. Decoding p53 tumor suppression: a crosstalk between genomic stability and epigenetic control? Cell Death and Differentiation. 2025; 32: 1–8. https://doi.org/10.1038/s41418-024-01259-9

[9] Zhao W, Zhang T, Hua X, Hoang PH, Miraftab M, Saha M, et al. A Prognostic Signature for Lung Adenocarcinoma in Patients Who Have Never Smoked. Cancer Discovery. 2026; 16: 460–477. https://doi.org/10.1158/2159-8290.CD-25-0581

[10] Kou YL, Liu YJ, Hsu TC, Wu KY, Chen ST, Chen JY, et al. SB431542, a Selective Inhibitor of the TGF-β Type I Receptor, Enhances Doxorubicin Antitumor Activity via p63 Activation in Mutant p53 Breast Cancer Cells. Frontiers in Bioscience (Landmark Edition). 2025; 30: 45389. https://doi.org/10.31083/FBL45389

[11] Arora C, Matic M, Bisceglia L, Di Chiaro P, De Oliveira Rosa N, Carli F, et al. The landscape of cancer-rewired GPCR signaling axes. Cell Genomics. 2024; 4: 100557. https://doi.org/10.1016/j.xgen.2024.100557

[12] Sahani PA, Patra R, Dixit A. G protein-coupled receptors (GPCRs) in cancer prognosis and therapeutics: A comprehensive review. International Journal of Biological Macromolecules. 2025; 328: 147665. https://doi.org/10.1016/j.ijbiomac.2025.147665

[13] Maparu K, Chatterjee D, Kaur R, Kalia N, Kuwar OK, Attri M, et al. Molecular crosstalk between GPCR and receptor tyrosine-protein kinase in neuroblastoma: molecular mechanism and therapeutic implications. Medical Oncology (Northwood, London, England). 2025; 42: 131. https://doi.org/10.1007/s12032-025-02685-6

[14] Ahn S, Kaipparettu BA. G-protein coupled receptors in metabolic reprogramming and cancer. Pharmacology & Therapeutics. 2025; 270: 108849. https://doi.org/10.1016/j.pharmthera.2025.108849

[15] Prossnitz ER, Barton M. The G protein-coupled oestrogen receptor GPER in health and disease: an update. Nature Reviews. Endocrinology. 2023; 19: 407–424. https://doi.org/10.1038/s41574-023-00822-7

[16] Lorente JS, Sokolov AV, Ferguson G, Schiöth HB, Hauser AS, Gloriam DE. GPCR drug discovery: new agents, targets and indications. Nature Reviews. Drug Discovery. 2025; 24: 458–479. https://doi.org/10.1038/s41573-025-01139-y

[17] Maudsley S, Schrauwen C, Harputluoğlu İ, Walter D, Leysen H, McDonald P. GPR19 Coordinates Multiple Molecular Aspects of Stress Responses Associated with the Aging Process. International Journal of Molecular Sciences. 2023; 24: 8499. https://doi.org/10.3390/ijms24108499

[18] Kastner S, Voss T, Keuerleber S, Glöckel C, Freissmuth M, Sommergruber W. Expression of G protein-coupled receptor 19 in human lung cancer cells is triggered by entry into S-phase and supports G(2)-M cell-cycle progression. Molecular Cancer Re-

search: MCR. 2012; 10: 1343–1358. https://doi.org/10.1158/1541-7786.MCR-12-0139
[19] Rao A, Herr DR. G protein-coupled receptor GPR19 regulates E-cadherin expression and invasion of breast cancer cells. Biochimica et Biophysica Acta. Molecular Cell Research. 2017; 1864: 1318–1327. https://doi.org/10.1016/j.bbamcr.2017.05.001
[20] Song B, Wang K, Peng Y, Zhu Y, Cui Z, Chen L, et al. Combined signature of G protein-coupled receptors and tumor microenvironment provides a prognostic and therapeutic biomarker for skin cutaneous melanoma. Journal of Cancer Research and Clinical Oncology. 2023; 149: 18135–18160. https://doi.org/10.1007/s00432-023-05486-4
[21] Aquino-Acevedo AN, Orengo-Orengo JA, Cruz-Robles ME, Saavedra HI. Mitotic kinases are emerging therapeutic targets against metastatic breast cancer. Cell Division. 2024; 19: 21. https://doi.org/10.1186/s13008-024-00125-x
[22] Glaviano A, Singh SK, Lee EHC, Okina E, Lam HY, Carbone D, et al. Cell cycle dysregulation in cancer. Pharmacological Reviews. 2025; 77: 100030. https://doi.org/10.1016/j.pharmr.2024.100030
[23] Rivas V, González-Muñoz T, Albitre Á, Lafarga V, Delgado-Arévalo C, Mayor F, Jr, et al. GRK2-mediated AKT activation controls cell cycle progression and G2 checkpoint in a p53-dependent manner. Cell Death Discovery. 2024; 10: 385. https://doi.org/10.1038/s41420-024-02143-8
[24] Tian J, Liu S, Zhang Y, Jia H, Nie W, Yang R, et al. LIMK2 promotes centrosome clustering and cancer progression by activating MST4-mediated phosphorylation of NPM1. Oncogene. 2025; 44: 3625–3639. https://doi.org/10.1038/s41388-025-03518-6
[25] Khan IR, Khurshid S, Almawash S, Kumar R, Akil ASAS, Bhat AA, et al. G Protein-Coupled Receptor Signaling: Implications and Therapeutic Development Advances in Cancers. MedComm. 2025; 6: e70375. https://doi.org/10.1002/mco2.70375
[26] Timofeev O, Giron P, Lawo S, Pichler M, Noeparast M. ERK pathway agonism for cancer therapy: evidence, insights, and a target discovery framework. NPJ Precision Oncology. 2024; 8: 70. https://doi.org/10.1038/s41698-024-00554-5
[27] Khan MA, Khan P, Ahmad A, Fatima M, Nasser MW. FOXM1: A small fox that makes more tracks for cancer progression and metastasis. Seminars in Cancer Biology. 2023; 92: 1–15. https://doi.org/10.1016/j.semcancer.2023.03.007
[28] Battistini C, Kenny HA, Zambuto M, Nieddu V, Melocchi V, Decio A, et al. Tumor microenvironment-induced FOXM1 regulates ovarian cancer stemness. Cell Death & Disease. 2024; 15: 370. https://doi.org/10.1038/s41419-024-06767-7
[29] Tan XQ, Guo AY, Zheng LF, Xiong J. Research progress on FOXM1 in ovarian cancer diagnosis and therapeutics. Frontiers in Oncology. 2025; 15: 1598868. https://doi.org/10.3389/fonc.2025.1598868
[30] Dilmac S, Hamurcu Z, Ozpolat B. Therapeutic Landscape of FOXM1 in Triple-Negative Breast Cancer and Aggressive Solid Cancers. Cancers. 2024; 16: 3823. https://doi.org/10.3390/cancers16223823
[31] Katzenellenbogen BS, Guillen VS, Katzenellenbogen JA. Targeting the oncogenic transcription factor FOXM1 to improve outcomes in all subtypes of breast cancer. Breast Cancer Research: BCR. 2023; 25: 76. https://doi.org/10.1186/s13058-023-01675-8
[32] Marvalim C, Datta A, Lee SC. Role of p53 in breast cancer progression: An insight into p53 targeted therapy. Theranostics. 2023; 13: 1421–1442. https://doi.org/10.7150/thno.81847
[33] Liao Y, Smyth GK, Shi W. featureCounts: an efficient general purpose program for assigning sequence reads to genomic features. Bioinformatics (Oxford, England). 2014; 30: 923–930. https://doi.org/10.1093/bioinformatics/btt656
[34] Love MI, Huber W, Anders S. Moderated estimation of fold change and dispersion for RNA-seq data with DESeq2. Genome Biology. 2014; 15: 550. https://doi.org/10.1186/s13059-014-0550-8
[35] Hertel A, Storchová Z. The Role of p53 Mutations in Early and Late Response to Mitotic Aberrations. Biomolecules. 2025; 15: 244. https://doi.org/10.3390/biom15020244
[36] McNeely SC, Xu X, Taylor BF, Zacharias W, McCabe MJ, Jr, States JC. Exit from arsenite-induced mitotic arrest is p53 dependent. Environmental Health Perspectives. 2006; 114: 1401–1406. https://doi.org/10.1289/ehp.8969
[37] Lok GTM, Chan DW, Liu VWS, Hui WWY, Leung THY, Yao KM, et al. Aberrant activation of ERK/FOXM1 signaling cascade triggers the cell migration/invasion in ovarian cancer cells. PloS One. 2011; 6: e23790. https://doi.org/10.1371/journal.pone.0023790
[38] Sadasivam S, Duan S, DeCaprio JA. The MuvB complex sequentially recruits B-Myb and FoxM1 to promote mitotic gene expression. Genes & Development. 2012; 26: 474–489. https://doi.org/10.1101/gad.181933.111
[39] Bi Z, Li H, Liang Y, Sun D, Liu S, Chen W, et al. Emerging paradigms for target discovery of traditional medicines: A genome-wide pan-GPCR perspective. Innovation (Cambridge (Mass.)). 2025; 6: 100774. https://doi.org/10.1016/j.xinn.2024.100774
[40] Zhang M, Chen T, Lu X, Lan X, Chen Z, Lu S. G protein-coupled receptors (GPCRs): advances in structures, mechanisms, and drug discovery. Signal Transduction and Targeted Therapy. 2024; 9: 88. https://doi.org/10.1038/s41392-024-01803-6
[41] Qin R, Fan X, Huang Y, Duan Y, Wang H. G protein-coupled receptors: pivotal hubs in gastric cancer malignancy-from multidimensional crosstalk to precision therapeutics. Journal of Translational Medicine. 2025; 23: 879. https://doi.org/10.1186/s12967-025-06851-2
[42] Lee YJ, Shin KJ, Jang HJ, Ryu JS, Lee CY, Yoon JH, et al. GPR143 controls ESCRT-dependent exosome biogenesis and promotes cancer metastasis. Developmental Cell. 2023; 58: 320–334.e8. https://doi.org/10.1016/j.devcel.2023.01.006
[43] Stelcer E, Milecka P, Komarowska H, Jopek K, Tyczewska M, Szyszka M, et al. Adropin Stimulates Proliferation and Inhibits Adrenocortical Steroidogenesis in the Human Adrenal Carcinoma (HAC15) Cell Line. Frontiers in Endocrinology. 2020; 11: 561370. https://doi.org/10.3389/fendo.2020.561370
[44] Klatt W, Wallner S, Brochhausen C, Stolwijk JA, Schreml S. Expression profiles of proton-sensing G-protein coupled receptors in common skin tumors. Scientific Reports. 2020; 10: 15327. https://doi.org/10.1038/s41598-020-71700-9
[45] Harding SD, Armstrong JF, Faccenda E, Southan C, Alexander SPH, Davenport AP, et al. The IUPHAR/BPS Guide to PHARMACOLOGY in 2024. Nucleic Acids Research. 2024; 52: D1438–D1449. https://doi.org/10.1093/nar/gkad944
[46] Stein LM, Yosten GLC, Samson WK. Adropin acts in brain to inhibit water drinking: potential interaction with the orphan G protein-coupled receptor, GPR19. American Journal of Physiology. Regulatory, Integrative and Comparative Physiology. 2016; 310: R476–R480. https://doi.org/10.1152/ajpregu.00511.2015
[47] Husted AS, Trauelsen M, Rudenko O, Hjorth SA, Schwartz TW. GPCR-Mediated Signaling of Metabolites. Cell Metabolism. 2017; 25: 777–796. https://doi.org/10.1016/j.cmet.2017.03.008
[48] Weis WI, Kobilka BK. The Molecular Basis of G Protein-Coupled Receptor Activation. Annual Review of Biochemistry. 2018; 87: 897–919. https://doi.org/10.1146/annurev-biochem-060614-033910
[49] D'Alessandre NDR, Pessoa BS, Guardia GDA, Marques JM,

Galante PAF, Batista RL. Retroelements in thyroid cancer: epigenetic plasticity, dedifferentiation, and therapeutic opportunities. Reviews in Endocrine & Metabolic Disorders. 2026; 27: 153–165. https://doi.org/10.1007/s11154-025-10008-3

[50] Gourisankar S, Krokhotin A, Ji W, Liu X, Chang CY, Kim SH, et al. Rewiring cancer drivers to activate apoptosis. Nature. 2023; 620: 417–425. https://doi.org/10.1038/s41586-023-06348-2

[51] Suvac A, Ashton J, Bristow RG. Tumour hypoxia in driving genomic instability and tumour evolution. Nature Reviews. Cancer. 2025; 25: 167–188. https://doi.org/10.1038/s41568-024-00781-9

[52] Kwon Y, Mehta S, Clark M, Walters G, Zhong Y, Lee HN, et al. Non-canonical β-adrenergic activation of ERK at endosomes. Nature. 2022; 611: 173–179. https://doi.org/10.1038/s41586-022-05343-3

[53] Pardo-Pastor C, Rosenblatt J. Piezo1 activates noncanonical EGFR endocytosis and signaling. Science Advances. 2023; 9: eadi1328. https://doi.org/10.1126/sciadv.adi1328

[54] Zerbib J, Ippolito MR, Eliezer Y, De Feudis G, Reuveni E, Savir Kadmon A, et al. Human aneuploid cells depend on the RAF/MEK/ERK pathway for overcoming increased DNA damage. Nature Communications. 2024; 15: 7772. https://doi.org/10.1038/s41467-024-52176-x

[55] Chan DW, Hui WW, Cai PC, Liu MX, Yung MM, Mak CS, et al. Targeting GRB7/ERK/FOXM1 signaling pathway impairs aggressiveness of ovarian cancer cells. PloS One. 2012; 7: e52578. https://doi.org/10.1371/journal.pone.0052578

[56] Ma RY, Tong TH, Cheung AM, Tsang AC, Leung WY, Yao KM. Raf/MEK/MAPK signaling stimulates the nuclear translocation and transactivating activity of FOXM1c. Journal of Cell Science. 2005; 118: 795–806. https://doi.org/10.1242/jcs.01657

[57] Ling Q, Meng C, Chen Q, Xing D. Activated ERK/FOXM1 pathway by low-power laser irradiation inhibits UVB-induced senescence through down-regulating p21 expression. Journal of Cellular Physiology. 2014; 229: 108–116. https://doi.org/10.1002/jcp.24425

[58] Noonan ML, Muto Y, Yoshimura Y, Leckie-Harre A, Wu H, Kalinichenko VV, et al. Injury-induced Foxm1 expression in the mouse kidney drives epithelial proliferation by a cyclin F-dependent mechanism. JCI Insight. 2024; 9: e175416. https://doi.org/10.1172/jci.insight.175416

[59] Yang Y, Liao J, Pan Z, Meng J, Zhang L, Shi W, et al. Dual Inhibition of CDK4/6 and CDK7 Suppresses Triple-Negative Breast Cancer Progression via Epigenetic Modulation of SREBP1-Regulated Cholesterol Metabolism. Advanced Science (Weinheim, Baden-Wurttemberg, Germany). 2025; 12: e2413103. https://doi.org/10.1002/advs.202413103

[60] Wei J, Chen X, Li Y, Li R, Bao K, Liao L, et al. Cucurbitacin B-induced G2/M cell cycle arrest of conjunctival melanoma cells mediated by GRP78-FOXM1-KIF20A pathway. Acta Pharmaceutica Sinica. B. 2022; 12: 3861–3876. https://doi.org/10.1016/j.apsb.2022.05.021

[61] Jin X, He X, Huang R, Liu Q, Wang L, Bai X, et al. SNRPB/CCNB1 axis promotes hepatocellular carcinoma progression and cisplatin resistance through enhancing lipid metabolism reprogramming. Journal of Experimental & Clinical Cancer Research: CR. 2025; 44: 211. https://doi.org/10.1186/s13046-025-03463-y

[62] Xu R, Lee YJ, Kim CH, Min GH, Kim YB, Park JW, et al. Invasive FoxM1 phosphorylated by PLK1 induces the polarization of tumor-associated macrophages to promote immune escape and metastasis, amplified by IFITM1. Journal of Experimental & Clinical Cancer Research: CR. 2023; 42: 302. https://doi.org/10.1186/s13046-023-02872-1

[63] Fischer M, Grossmann P, Padi M, DeCaprio JA. Integration of TP53, DREAM, MMB-FOXM1 and RB-E2F target gene analyses identifies cell cycle gene regulatory networks. Nucleic Acids Research. 2016; 44: 6070–6086. https://doi.org/10.1093/nar/gkw523

[64] Junk DJ, Vrba L, Watts GS, Oshiro MM, Martinez JD, Futscher BW. Different mutant/wild-type p53 combinations cause a spectrum of increased invasive potential in nonmalignant immortalized human mammary epithelial cells. Neoplasia (New York, N.Y.). 2008; 10: 450–461. https://doi.org/10.1593/neo.08120

[65] Leroy B, Girard L, Hollestelle A, Minna JD, Gazdar AF, Soussi T. Analysis of TP53 mutation status in human cancer cell lines: a reassessment. Human Mutation. 2014; 35: 756–765. https://doi.org/10.1002/humu.22556